UNCERTAINTY ANALYSIS OF INTEGRATED POWERHEAD DEMONSTRATOR MASS FLOWRATE TESTING AND MODELING

By

King Jeffries Molder

A Thesis
Submitted to the Faculty of
Mississippi State University
in Partial Fulfillment of the Requirements
for the Degree of Master of Science
in Mechanical Engineering
in the Department of Mechanical Engineering

Mississippi State, Mississippi

August 2005

UNCERTAINTY ANALYSIS OF INTEGRATED POWERHEAD DEMONSTRATOR MASS FLOWRATE TESTING AND MODELING

By

King Jeffries Molder

Approved:

W. Glenn Steele Professor and Head of the Department of Mechanical Engineering (Director of Thesis)	Susan T. Hudson Adjunct Assistant Professor of Mechanical Engineering (Committee Member)
Louay M. Chamra Associate Professor of Mechanical Engineering (Committee Member)	Steven R. Daniewicz Professor and Graduate Coordinator of the Department of Mechanical Engineering
Kirk H. Schulz Professor and Dean of the Bagley College of Engineering	

Name: King Jeffries Molder

Date of Degree: August 6, 2005

Institution: Mississippi State University

Major Field: Mechanical Engineering

Major Professor: Dr. W. Glenn Steele

Title of Study: UNCERTAINTY ANALYSIS OF INTEGRATED POWERHEAD DEMONSTRATOR MASS FLOWRATE TESTING AND MODELING

Pages in Study: 59

Candidate for Degree of Master of Science

A methodology has been developed to quantify the simulation uncertainty of a computational model calibrated against test data. All test data used in the study undergoes an experimental uncertainty analysis. The modeling software ROCETS is used and its structure is explained. The way the model was calibrated is presented. Next, a general simulation uncertainty analysis methodology is shown that is valid for calibrated models. Finally the ROCETS calibrated model and its simulation uncertainty are calculated using the general methodology and compared to a second set of comparison test data. The simulation uncertainty analysis methodology developed and implemented can be used for any modeling with a calibrated model. The methodology works well for a process of incremental testing and recalibration of the model whenever new test data is available.

ACKNOWLEDGMENTS

I would like to dedicate this research to my parents, Rick and Deborah Molder, and my brother Chaz. I would also like to thank my major professor Dr. Glenn Steele for his help throughout my time at Mississippi State and my advisory committee members Dr. Louay Chamra and Dr. Susan Hudson. Finally, I would like to thank the folks at NASA Marshall and NASA Stennis, namely Tom Giel and Paul Rieder for their help with my questions and obtaining the modeling and testing information.

TABLE OF CONTENTS

CHAPTER Page

LIST OF TABLES

LIST OF FIGURES

FIGURE Page

CHAPTER I

INTRODUCTION

Uncertainty analysis has permeated throughout the aerospace industry and has become an integral component of rocket engine testing. The planning of testing has become more efficient through the use of uncertainty analysis, and project managers have more confidence in their test results because of uncertainty analysis. While these great strides with uncertainty analysis have been made in testing, very little progress has been made in using uncertainty analysis as a tool in rocket engine modeling. Modeling is an important part of any design and testing process due to the reduction of risk for the test article. Therefore, the ability to improve modeling through uncertainty analysis will positively impact the testing and test article.

1.1 Background

The focus of this work is on the Integrated Powerhead Demonstrator (IPD). The IPD is a joint venture between NASA and the U.S. Air Force that hopes to develop engine technologies that could, within decades, power the next generation of space transportation [1]. The project is the first full-scale effort to develop a full-flow, hydrogen-fueled, staged-combustion rocket engine in the 250,000 pound thrust class. The IPD engine employs dual preburners that provide both oxygen-rich and hydrogen-rich staged combustion. This innovative approach is expected to keep engine

components cooler during flight leading to increased reliability while achieving the highest efficiency by using all propellant flow.

The IPD project addresses two major technology challenges which are turbine life and bearing wear. These two technologies have limited the performance of rocket engines in the past. By sending all of the propellant flow through the turbine, the same amount of energy can be extracted with a lower temperature gas which reduces the likelihood of material fatigue caused by sustained high temperatures. The IPD turbomachinery includes revolutionary hydrostatic bearings that fully support the rotor of both the fuel and oxidizer pumps. Because the hydrostatic bearings actually cause the rotor to float on a layer of liquid during operation, bearing wear only occurs for a few seconds during engine startup and shutdown.

The testing of the IPD is being conducted in the E-1 test stand at the NASA Stennis Space Center. The modeling for the IPD program is being done at the NASA Marshall Space Flight Center. The major components of the IPD were developed for NASA and the Air Force by Boeing Rocketdyne and the Aerojet Corporation. Due to the International Traffic in Arms Regulations (ITAR), some technologies of the IPD cannot be discussed. The ITAR restrictions also apply to all testing and modeling data discussed in subsequent chapters.

1.2 Objective

The ability to accurately measure transient cryogenic flow is critical to the success of the IPD project. One of the largest risks to starting the engine will be the understanding of the actual mixture ratio of the engine as it undergoes the startup and

shutdown phases of operation. To reduce this risk, uncertainty analysis methodologies are needed to asses the uncertainty associated with the computational modeling and testing of IPD. Once these methodologies are implemented, they should quantify the uncertainties associated with the modeling and testing. The specific IPD parameters of interest are the liquid oxygen system (LOX) and liquid hydrogen system (LH2) mass flowrates as measured by venturi flow meters.

This study examines the uncertainty of the IPD activation testing and modeling efforts. The experimental uncertainty analysis done on the Stennis facility will provide methodology that can be applied to future testing using venturi flow meters. The uncertainty analysis of the Marshall modeling process will create a general framework for use on any model that is calibrated specifically by comparison with test data. The general modeling uncertainty framework will then been adapted to fit the modeling for IPD.

There were four IPD activation tests examined in the study. Activation tests occur at a test installation before the test article has been installed. The purpose of the activation tests is to make sure the facility can handle the upcoming test article safely. Tests 19A and 19D were tests of the LH2 system and used liquid hydrogen as the test fluid. Test 9B and 10C were tests of the LOX system. Test 9B used liquid nitrogen as the test fluid and test 10C used liquid oxygen as the test fluid. The LH2 tests were approximately sixty seconds in duration while the LOX system tests were approximately twenty seconds in duration.

The experimental uncertainty analysis methodology and implementation for IPD are developed and discussed in the first part of this study. Then a description of the IPD

modeling effort is given. Next the uncertainty methodology for a calibrated model is introduced. Finally, experimental data and model data are used to demonstrate the newly developed model uncertainty methodology.

CHAPTER II

LITERATURE REVIEW

The focus of this literature review was on previous work conducted on model uncertainty analysis. Experimental uncertainty analysis was also reviewed since it is a basis from which most modeling uncertainty is derived. In general, modeling uncertainty exists due to numerical accuracy and simplifying assumptions and to variations in design conditions, input parameters, and other components of a model. Most of the literature on modeling uncertainty has addressed the effect of input parameter uncertainty. Some recent work has addressed the area of verification and validation (V&V) in an attempt to estimate the other components of model uncertainty.

The basis for modeling uncertainty was adapted from the widely used experimental uncertainty analysis. The experimental uncertainty analysis references for this study all use the same basic methodology. The worldwide standard for this experimental uncertainty analysis is authored by the International Organization for Standardization [2]. The American Society of Mechanical Engineers publishes the American standard for experimental uncertainty analysis [3]. Coleman and Steele's book on experimentation and uncertainty analysis is a good reference for many different applications of experimental uncertainty analysis [4]. Coleman and Steele's latest work

on general experimental uncertainty analysis updates the nomenclature from their earlier work [5].

The journal articles reviewed for this study agree that uncertainties existing in any computational simulation are greatly affected by the input parameter uncertainties. To determine to what degree each input affects the model, a sensitivity analysis must be done. Taylor et al. conducted a study on a piping system design model that used the inputs' uncertainty to quantify a model's uncertainty [6]. Later Taylor et al. worked with diffuse-gray radiation enclosure problems which again exercised a sensitivity analysis and input parameter uncertainty to estimate a model result uncertainty. Taylor also conducted an extensive literature search on sensitivity analysis related to modeling [7].

The American Institute of Aeronautics and Astronautics (AIAA) defines verification as the process of determining that a model implementation accurately represents the developer's conceptual description of the model and the solution to the model. AIAA defines validation as the process of determining the degree to which a computer model is an accurate representation of the real world from the perspective of the intended model applications [8]. Coleman's paper states that Roache defines verification as solving the equations right and validation as solving the right equations [9]. Chamra et al. applies these definitions to validate a model in a study on the uncertainty associated with thermal comfort [10]. The most recent example of the application of V & V was done by Mago et al. in a study on a model for the performance of a hybrid liquid desiccant system during cooling and dehumidification [11]. Validation and its uncertainty is an essential part of the simulation uncertainty methodology

discussed later in this study. The AIAA has developed a general guide for the verification and validation process [8]. Also the American Society of Mechanical Engineers has a committee developing a detailed guide for verification and validation in computational fluid dynamics and heat transfer [12].

The big question for any simulation effort is how well the model predicts a validation experimental test result. From Coleman and Stern, comparison error is introduced as the resultant of all the errors associated with the experimental data and the errors associated with the simulation [13]. The comparison error assumes that a correction has been made for any error whose value is known.

Based on the literature survey there is a general consensus on the sources of simulation uncertainty as discussed at the beginning of this section. There is also a consensus on the definition of verification and validation. There are, however, different methods to quantify the verification and validation. This study will use a variation on the validation process from Coleman and Stern. The definitions and terminology discussed above will be used to build a simulation uncertainty methodology appropriate for the calibrated model used in this study.

CHAPTER III

EXPERIMENTAL UNCERTAINTY ANALYSIS

The experimental data used in this study was activation data. Activation is the process through which a facility is tested and checked for problems before a test article is installed. The facility included the LOX and LH2 run tanks to supply the test liquids and the supply piping from the tanks to the test article interface. The supply piping included the venturis to measure the mass flowrates and many other purge valves and bleed valves. A pneumatically controlled butterfly valve was used to represent the IPD test article at the test article interface during the activation tests. The run tanks from which the test liquids flowed kept a near constant pressure throughout each test. Therefore, the butterfly valves controlled the flow for each system. The rest of the chapter will discuss how the mass flowrates were measured, present the experimental results from the activation tests, and consider the uncertainty for each test.

3.1 Background

The parameters of interest for this study are the LOX system mass flowrate and LH2 system mass flowrate of the Integrated Powerhead Demonstrator activation tests. Both of these flowrates are measured by their respective venturi flow meters. A venturi is a device to measure flowrate of a fluid in a pipe. Venturi flow meters are often used to

measure fluid flow due to their low permanent pressure loss, durability, and lack of moving parts.

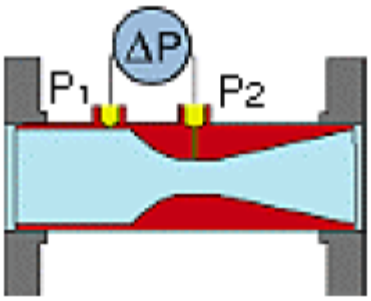

Figure 3.1 Schematic of Venturi Flow Meter

As shown in Figure 3.1, venturis are part of a class of flow meters known as differential pressure measurement devices since a pressure drop across a region in the meter is produced, and this pressure differential is used to determine the flowrate through the meter. The area is reduced and the velocity is increased at the venturi throat. The venturi volumetric flowrate, WPUMP, used for this study is given as equation (3-1). WPUMP is the name used by NASA for the mass flowrate.

$$WPUMP = .52502 C_d D_T^2 F \sqrt{\frac{\rho \Delta P}{1-\beta^4}} \tag{3-1}$$

where

$$\beta = \frac{D_T}{D_I} \tag{3-2}$$

Here C_d is the dimensionless discharge coefficient and D_T is the diameter of the venturi throat. A thermal expansion factor, F, is needed to account for the expansion and

contraction of most materials as their temperature increases or decreases. The differential pressure measurement is represented by ΔP. The density of the fluid entering the venturi is ρ. The ratio of the venturi throat diameter, D_T, to the venturi inlet diameter, D_I, is the β given in equation (3-2). WPUMP will result in a mass flowrate with units in lb_m/sec. The inputs and their required units for input into the WPUMP equation are listed in Table 3.1.

Table 3.1 WPUMP Parameters

Parameter	Units	Description
C_d	NA	venturi discharge coefficient
F	NA	thermal expansion factor of venturi material
D_T	inches	venturi throat diameter
D_I	inches	venturi inlet diameter
ρ	lbm/ft^3	fluid density
ΔP	psid	pressure difference across venturi measured directly
.52502	NA	factor including all conversions for units

An overview of experimental uncertainty analysis is given in the next section to illustrate the methodology used to determine the mass flowrate uncertainty.

3.2 Experimental Uncertainty Overview

The methodology for applying uncertainty analysis to an experimental result is summarized below, from Steele and Coleman's "Experimental Uncertainty Analysis," in the *CRC Handbook of Mechanical Engineering*, 2nd edition, 2005 [5]. In nearly all experiments, the measured values of different variables are combined using a data

reduction equation (DRE) to form some desired result. A general representation of a data reduction equation is

$$r = r(X_1, X_2, ..., X_J) \tag{3-3}$$

where r is the experimental result determined from J measured variables X_i. Each of the measured variables contains systematic (fixed) errors and random (varying) errors. These errors in the measured values then propagate through the DRE, thereby generating the systematic and random errors in the experimental result, r. Uncertainty analysis is used to estimate the random and systematic standard uncertainties of the result, s_r and b_r, respectively, and the corresponding expanded uncertainty of the result, U_r.

If it is assumed that the degrees of freedom for the result is large (>10), which is very appropriate for most engineering applications, then the "large sample assumption" applies, and the 95% confidence expression for U_r is

$$U_r = 2\sqrt{b_r^2 + s_r^2} \tag{3-4}$$

The systematic standard uncertainty of the result is defined as

$$b_r^2 = \sum_{i=1}^{J} \theta_i^2 b_i^2 + 2 \sum_{i=1}^{J-1} \sum_{k=i+1}^{J} \theta_i \theta_k b_{ik} \tag{3-5}$$

where

$$\theta_i = \frac{\partial r}{\partial X_i} \tag{3-6}$$

The systematic standard uncertainty estimate for each X_i variable is the root-sum-square combination of its elemental systematic standard uncertainties

$$b_i = \left[\sum_{j=1}^{M} b_{i_j}^2 \right]^{1/2} \tag{3-7}$$

where M is the number of elemental systematic standard uncertainties for X_i and where each b_{i_j} is the standard deviation level estimate of the systematic uncertainty in variable X_i resulting from error source j. The standard deviation level systematic uncertainty estimate for an error source is usually made by making a 95% confidence estimate of the limits of the error for that source and dividing that estimate by 2. The second term in equation (3-5) accounts for systematic errors that have the same source and are correlated. The factor b_{ik} is the covariance term appropriate for the systematic errors that are common between variables X_i and X_k and is determined as

$$b_{ik} = \sum_{\alpha=1}^{L} b_{i_\alpha} b_{k_\alpha} \tag{3-8}$$

where variables X_i and X_k share L identical systematic error sources. The random standard uncertainty of the result is defined as

$$s_r^2 = \sum_{i=1}^{J} \theta_i^2 s_i^2 \tag{3-9}$$

where s_i is the sample standard deviation for variable X_i (sample standard deviation of the mean if X_i is a mean value or sample standard deviation if X_i is a single reading).

3.3 Input Parameter Uncertainty

Each input parameter used in the mass flowrate equation contains a source of uncertainty that contributes to the overall uncertainty of WPUMP. These individual contributions propagate through the data reduction equation as discussed in the uncertainty overview section. The uncertainty contribution of each parameter will be discussed individually in the following paragraphs. Table 3.2, given at the end of this section, summarizes all input parameter sources of uncertainty.

The discharge coefficient, C_d, uncertainty was determined from calibration data provided by Colorado Engineering Experiment Station, Inc. (CEESI) to NASA Stennis. For both venturi flowmeters, CEESI quoted an overall mass flowrate uncertainty of .5% of reading. Using this quoted value as the uncertainty for WPUMP in the mass flowrate expression equation (3-1), the uncertainty of the calibration system ΔP, the uncertainties of the venturi dimensions, and the methodology in section 3.2, the uncertainty of C_d was determined for each venturi. The discharge coefficient for the LOX system venturi was .985 with an uncertainty of .00488. The discharge coefficient for the LH2 system venturi was .975 with an uncertainty of .00484.

The thermal expansion factor, F, is needed to take into account the expansion or contraction of the venturi material. It is used when the test temperature of the venturi is well outside standard room temperature. The thermal expansion factor was determined from information in *Fluid Meters: Their Theory and Application* [15]. This information is given as Figure 3.2. The material for the two venturis in this study is type 304L stainless steel, which falls in the 300 Series SS category. It was determined from Figure 3.2 that

.0005 would be a good estimate of F's uncertainty due to the difference between materials' expansion factor values at low temperatures. Once this uncertainty was applied, it was found that its effect on the uncertainty of mass flowrate was negligible when compared with the contributions from the other variables. Therefore, the uncertainty in F was not considered in the flowrate uncertainty for both systems.

The two measurements of the venturis' inner diameters are D_T and D_I, denoting the throat diameter and inlet diameter respectively. Both venturis were of the same dimensions and were installed before this study began. Since the venturis were already installed no direct measurements could be made. Therefore the tolerances from the engineering drawings were used to estimate the uncertainty in their measurement for both the LOX and LH2 venturis. The uncertainty from the tolerance was .001inches for the throat diameter. The inlet diameter tolerance gave an uncertainty of .01 inches.

The differential pressure measurement, ΔP, was the most dominant uncertainty contributor for the venturi flowrate. A spreadsheet from earlier work at Stennis was used to calculate the uncertainty of the pressure transducer [14]. This spreadsheet is given in Appendix A. Based on NASA Stennis procedures, there were three significant elemental error sources for the pressure transducer. The sources were transducer calibration from the calibration laboratory, key number calibration, and allowable drift after facility calibration. Key number uncertainty is a function of the pressure transducer's internal shunt resistance and its output during calibration [16]. Considering the sources of error for the pressure transducer, six user inputs were needed to calculate the systematic uncertainty utilizing the spreadsheet. The inputs were full-range scale of the transducer,

post-test check tolerance set by facility personnel, the gain set by facility personnel, uncertainty from the key number, what class of calibration the transducer underwent, and whether an absolute pressure was calculated on a differential pressure reading. Once the spreadsheet had the proper inputs, it was determined that both the LOX venturi transducer and the LH2 venturi transducer had an uncertainty of 1.21 psi.

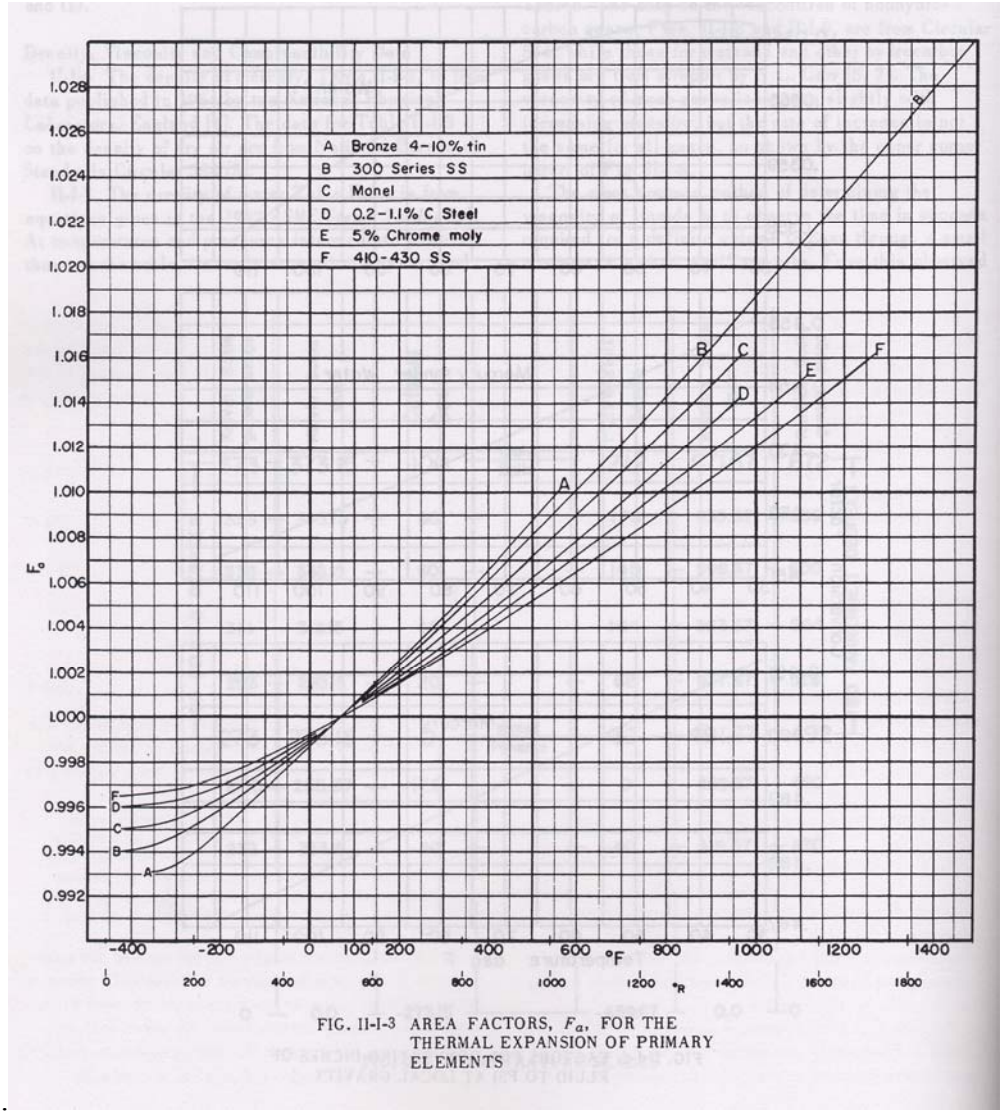

FIG. II-I-3 AREA FACTORS, F_a, FOR THE THERMAL EXPANSION OF PRIMARY ELEMENTS

Figure 3.2 Thermal Expansion Factor Plot

The density of the fluid entering the venturi was determined from a NIST table used by NASA Stennis in their data processing. The measurements needed to determine the density from the table were temperature and pressure of the fluid entering the venturi. A resistance temperature detector (RTD) and pressure transducer just upstream of the venturi were used to obtain these measurements. There was no direct access to the NIST program, therefore; previous work done to look at the sensitivity of the NIST program was reviewed. The previous work looked at variations of density over temperature and pressure ranges for typical tests. The temperature range dominated the variation of density from the NIST tables. It was determined from review of this information and the characteristic accuracy of NIST tables that 1% of the density value would be a good estimate of the density uncertainty for both the LOX and LH2 systems.

Table 3.2 Input Parameter Uncertainty Summary

Parameter	Units	LOX Uncertainty	LH2 Uncertainty
C_d	NA	.00488	.00484
F	NA	negligible	negligible
D_T	inches	.001 inches	.001 inches
D_I	inches	.01 inches	.01 inches
ρ	lb_m/ft^3	1.0%	1.0%
ΔP	psid	1.21 psi	1.21 psi

All of the input parameter uncertainties given in Table 3.2 are systematic. Random uncertainty, as stated before, is a varying error that accounts for variations in a measured parameter during the measurement process. The parameters C_D, F, D_T, and D_I are constant input values during the measurement process and, therefore, have no random

uncertainty. In general ρ could have random uncertainty from random uncertainties in the temperature and pressure measurements, but for these tests the random uncertainties were negligible. Also, the pressure drop, ΔP, can have random uncertainty because of the test conditions. The data for the activation tests showed oscillations in the venturi pressure drop data. It was determined that fluctuations in ΔP were caused by real oscillations in the mass flowrate and were not random in nature after consultation with NASA Stennis. Plots of the mass flowrates where the fluctuations can be seen are given in the next section. This being said, all uncertainty associated with the LOX system venturi and LH2 system venturi was considered to be systematic only.

Table 3.3 summarizes the flowrate uncertainty for each test fluid over a range of flowrates. The flowrates are fractions of the maximum flowrate seen by each system and the uncertainties are percent of the same maximum flowrate. Values for liquid nitrogen (LN) are given because this fluid was used as a substitute for LOX in some of the tests. The large uncertainty seen at the low flowrates was due to the uncertainty and range of the pressure transducers. At the points where the pressure measurements were closer to full scale, which is at the higher flowrates, the uncertainties reduced dramatically. To improve uncertainty at the low flow ranges, pressure transducers with a smaller measurement range would be needed.

Table 3.3 Venturi Mass Flowrate Uncertainty Summary

LN Flowrate	Uncertainty (%)	LOX Flowrate	Uncertainty (%)	LH2 Flowrate	Uncertainty (%)
.76+	1.70	.93+	2.00	.89+	2.80
.68 -.76	1.90	.84 -.93	2.10	.78 -.89	3.30
.59 -.68	2.10	.76 -.84	2.40	.67 -.78	3.90
.51 -.59	2.40	.68 -.76	2.60	.55 -.67	4.40
.42 -.51	2.90	.59 -.68	3.00	.44 -.55	5.50
.34 -.42	3.50	.51 -.59	3.50	.33 -.44	7.80
.25 -.34	4.70	.42 -.51	4.10	.22 -.33	11.1
.17 -.25	7.30	.34 -.42	5.10	.11 -.22	22.2
.12 -.17	10.1	.25 -.34	6.80	.09 -.11	29.9
.10 -.17	11.8	.17 -.25	10.6	.07 -.09	37.7
		.15 -.17	11.5	.04 -.07	55.5
				.02 -.04	110.9

3.4 Experimental Data

The four activation tests mentioned in the introductory chapter are examined in this section. Tests 19A and 19D were tests of the LH2 system and used liquid hydrogen as the test fluid. Test 9B and 10C were tests of the LOX system. Test 9B used liquid nitrogen as the test fluid and test 10C used liquid oxygen as the test fluid. The LH2 tests were approximately sixty seconds in duration while the LOX system tests were approximately twenty seconds in duration. The plots of each include the uncertainty bands for selected data points to show the nominal uncertainty of the test result. These selected points and their uncertainty bands show the trend of the uncertainty as the test progresses. If all points and their uncertainties were shown, the plot would become cluttered and unreadable. Separate plots of each test's transient section are shown because they were of special interest to NASA. Analysis of the activation data transient sections will help NASA to determine when to fire the IPD engine when the actual

engine tests are run. The plots are normalized due to the ITAR restrictions on the test data. The LOX system tests are normalized by one value and the LH2 system tests are normalized by another. LOX test 10C and LH2 test 19D are considered calibration tests in reference to modeling discussed later in this study. LOX test 9B and LH2 test 19A are considered comparison tests in reference to the modeling.

3.4.1 LH2 System Test 19D

LH2 system test 19D was run using the LH2 system and LH2 as the test liquid. The entire test length was sixty-three seconds as shown in Figure 3.3. It had a transient start-up of approximately five seconds occurring from time zero to time five seconds, which is shown in Figure 3.4. The maximum flowrate for this test was used to normalize all test data of the LH2 system.

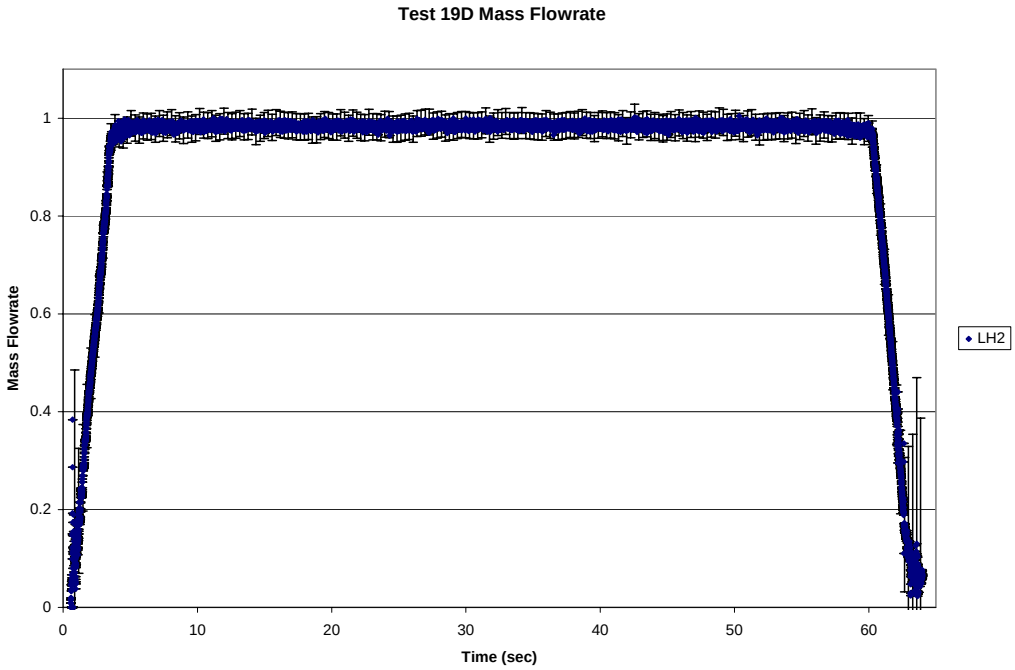

Figure 3.3 LH2 Test 19D

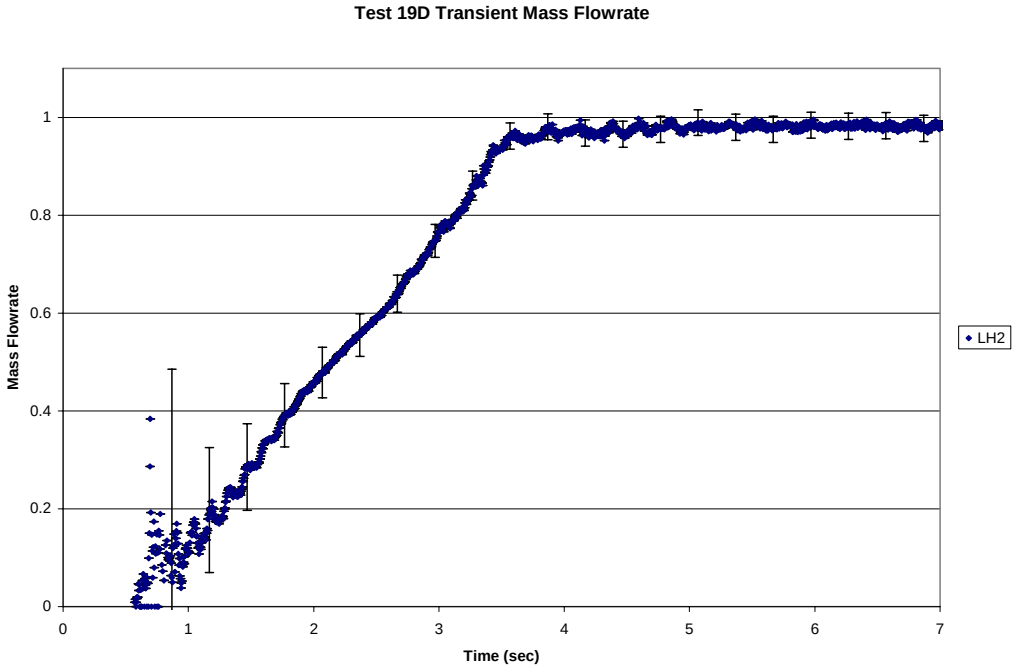

Figure 3.4 LH2 Test 19D Transient

3.4.2 LH2 System Test 19A

LH2 system test 19A was run using the LH2 system and LH2 as the test liquid. The entire test length was sixty-three seconds as shown in Figure 3.5. It had a transient start-up of approximately five seconds occurring from time zero to time five seconds, which is shown in Figure 3.6.

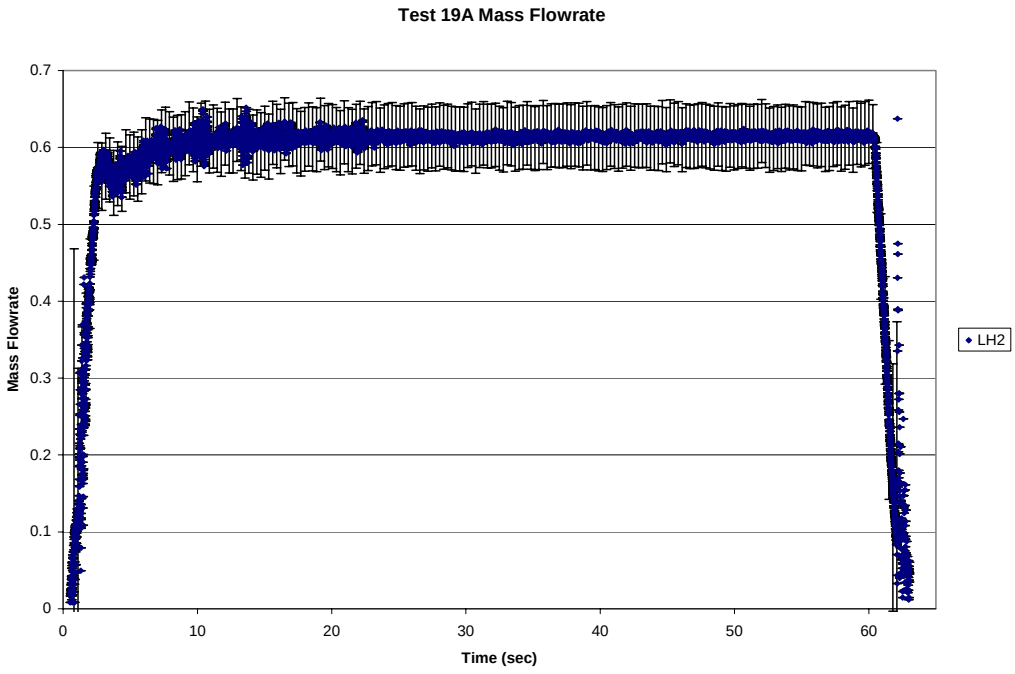

Figure 3.5 LH2 System Test 19A

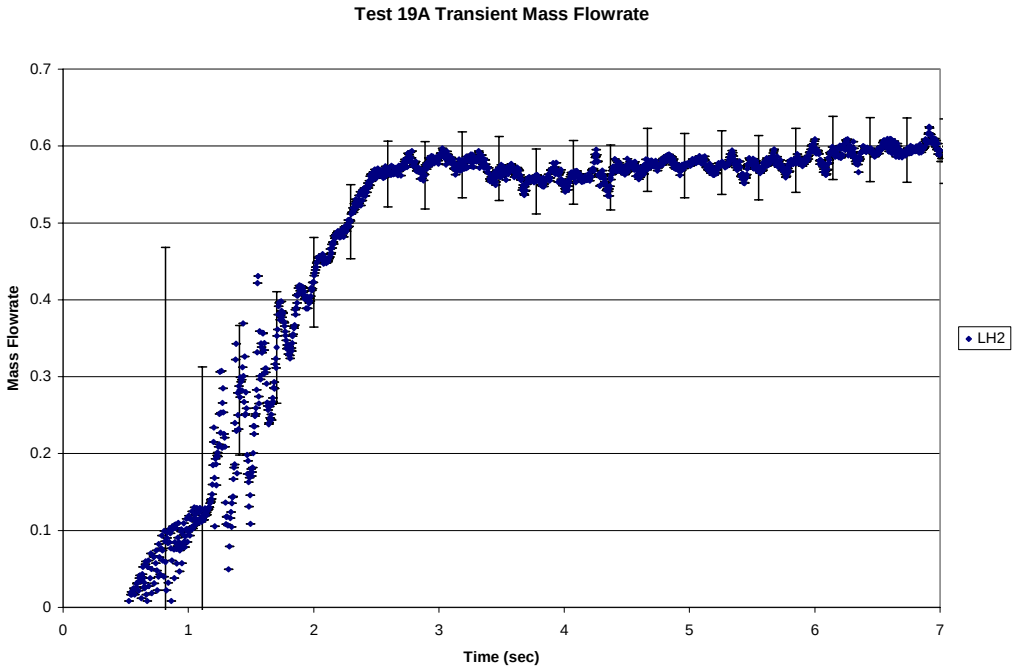

Figure 3.6 LH2 System Test 19A Transient

3.4.3 LOX System Test 10C

LOX system test 10C was run using the LOX system and LOX as the test liquid. The entire test length was twenty seconds as shown in Figure 3.7. It had a transient start-up of approximately two seconds occurring from time five seconds to time seven seconds, which is shown in Figure 3.8. The maximum flowrate for this test was used to normalize all test data of the LOX system.

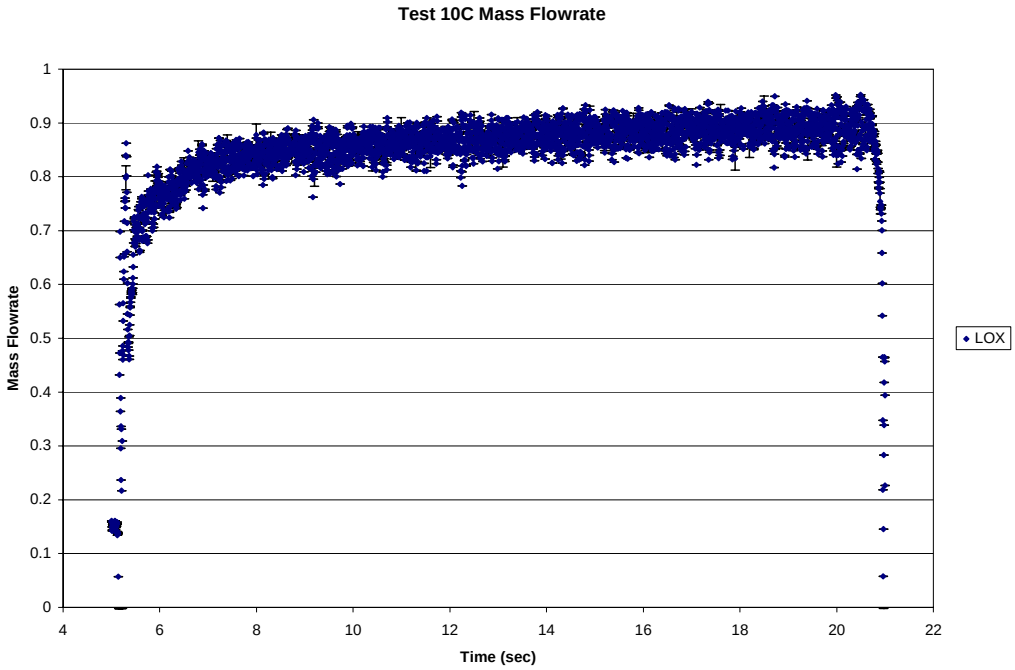

Figure 3.7 LOX System Test 10C

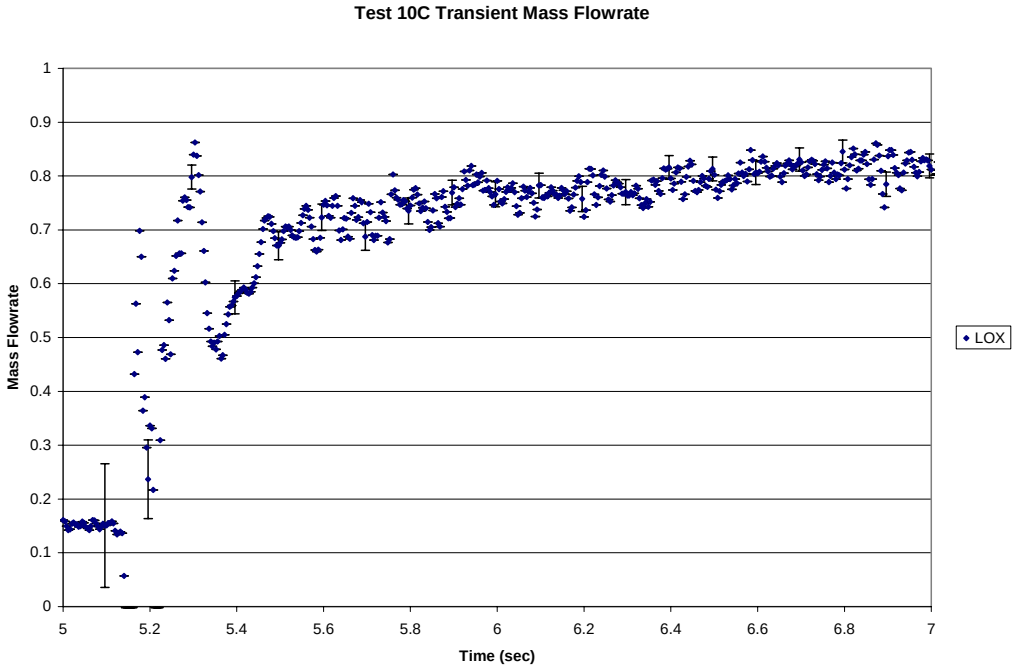

Figure 3.8 LOX System Test 10C Transient

3.4.4 LOX System Test 9B

LOX system test 9B was run using the LOX system and LN as the test liquid. The entire test length was twenty seconds as shown in Figure 3.9. It had a transient start-up of approximately two seconds occurring from time five seconds to time seven seconds, which is shown in Figure 3.10.

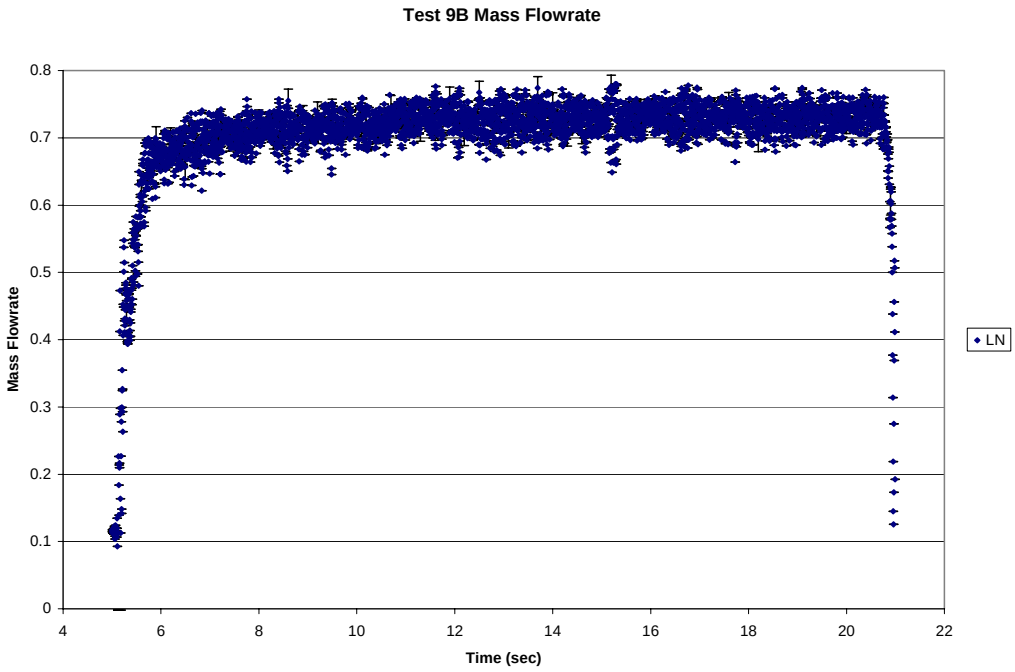

Figure 3.9 LOX System Test 9B

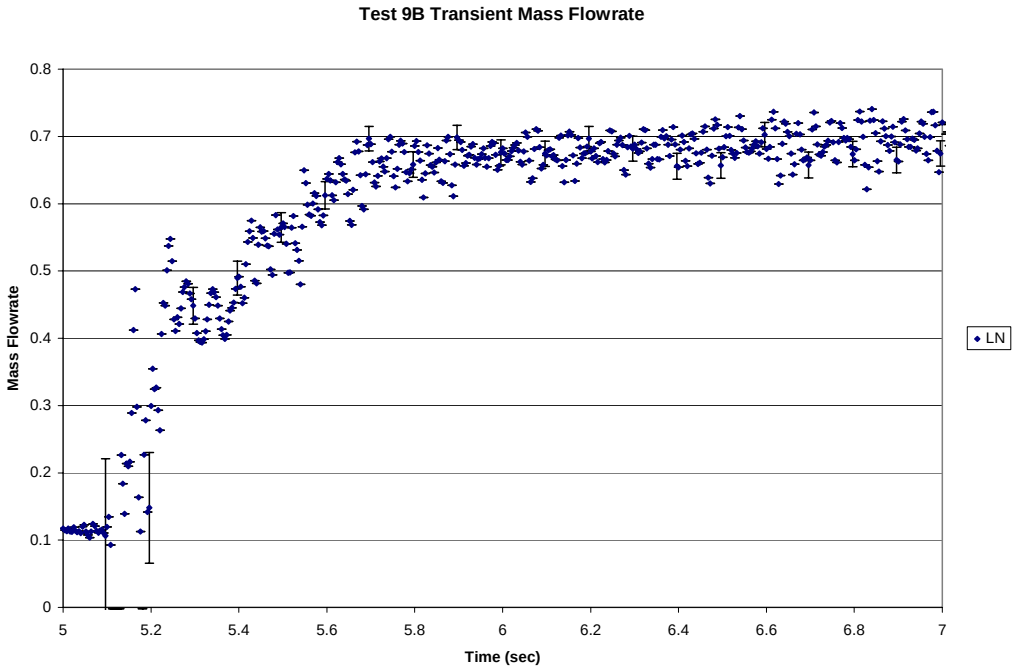

Figure 3.10 LOX System Test 9B Transient

CHAPTER IV

MODELING

4.1 ROCETS

The modeling program being used for IPD is ROCETS, which is an acronym for ROCket Engine Transient Simulation. The building of the ROCETS executable program was done by NASA Marshall. The structure of ROCETS makes it highly adaptable to simulate any type of rocket engine cycle with varying levels of modeling detail as desired by the user [17]. The goal of ROCETS is to aid the user in creating and using a simulation by automatically generating an executable model from input, scanning the model for undefined variables or variables which require algebraic loops, and supplying state-of-the-art numerical techniques.

The ROCETS system uses a configuration preprocessor to translate a user-supplied model description into a FORTRAN subroutine. This subroutine is then compiled and linked with module subroutines, property routines, and other runtime support routines to form an executable program. The modules are stand-alone, FORTRAN 77 subroutines that implement engineering equations to represent a particular engine component. Standard ROCETS modules are available in a library. Also users may modify these or create new model-specific modules as the problem requires.

NASA Marshall has created many of their own modules, some of which are included in the IPD model.

When the FORTRAN executable program is run, input data and execution control commands are interpreted from an input file. The results of the program are given in a solution file, output file, and plot file. The plot file was used in conjunction with the WinPlot program to examine the results for the purposes of this study. The solution file and output file were checked to make sure that solutions converged. A simple illustration of the program building process and its outputs is given in Figure 4.1.

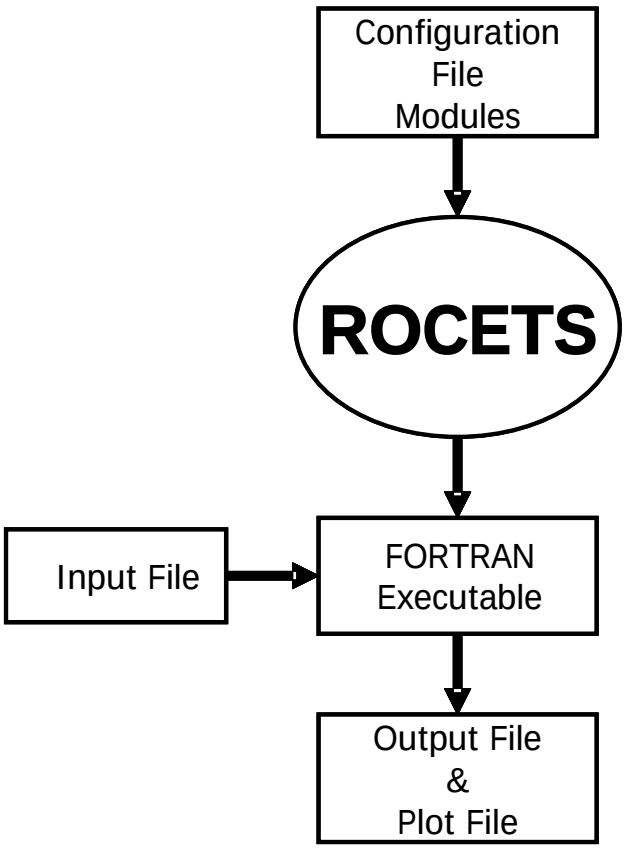

Figure 4.1 IPD Model Building Process

A schematic of the Stennis system modeled in this study is given as Figure 4.2. The overall ROCETS scheme is an iterative, multi-variable, Newton-Rahpson predictor-corrector equation solver. It starts with initial pressure and enthalpy guesses at the nodes to determine all needed fluid properties. Properties are defined at nodes, not in the legs connecting nodes. Then ROCETS calculates flows and flow derivatives in each leg from the leg's resistance value and fluid density. Next ROCETS predicts new node pressures and enthalpies to conserve mass, momentum, and energy within each volume. Newton-Rahpson iteration is performed to solve the set of the mass, momentum, and energy equations imbedded in the flow and volume modules representing the different system components. Iteration on the corrector continues at each time step until convergence to within a preselected tolerance of the variables is reached. If convergence is not attained within a preselected number of steps, the time step is reduced and iteration begins anew. Pressures, enthalpies, flowrates, etc., are determined at each time step in this manner to get to a solution. Then another time step is taken and the process repeats [18].

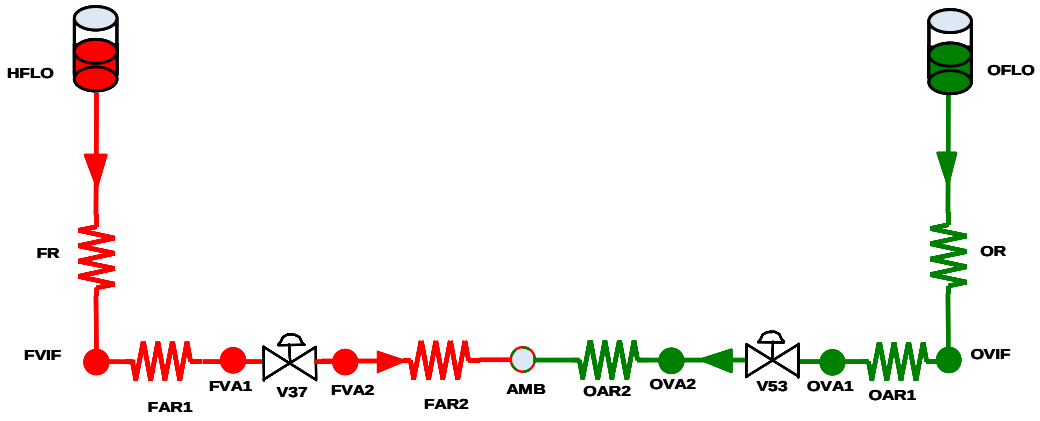

Figure 4.2 IPD Model Schematic

4.2 Model Calibration

A major part of the model building process for this NASA Marshall project was the use of what will be called a calibration run. The calibration run is test data used as an original anchor for the model. Once the executable is created and run, it is compared to the calibration run. Changes are made to the executable to match the calibration run at that point. These adjustments can include adding unrealistic conditions to the model just for the purpose of matching the calibration run. Since the model is anchored and adjusted in this manner, it is very specific to the test data of the calibration run and is primarily useful for predicting future test results for runs similar to the calibration run. The model may then not prove useful for predicting other tests that do not have very similar conditions.

This calibrated model process satisfies the needs of NASA Stennis and Marshall quite well because, after the original calibration run, the model is adjusted throughout a test series. Every time a new test is run, it becomes the new calibration run. The model continues to be tweaked during these comparisons. This process serves their purpose of slowly inching their way to a full-flow test while not damaging the test article being tested.

4.3 Sensitivity Analysis

4.3.1 Input File

A sensitivity analysis of the calibrated model inputs was done. The sensitivity analysis can help the model user to determine which inputs are most influential when

calibrating the model to the data. The inputs studied were located in the input file which controls each simulation. The input file consists of required information to set inputs, define balances, specify output, and control execution. Normally inputs for the input file come from desired design points for an upcoming test. However, in this case, inputs were taken from previous test data. The analysis of the model was not concerned with most of the commands of the input file, but there were five sections utilized in the sensitivity analysis. The first of the five sections used conditions from full-flow test data to determine steady-state line resistances and valve settings at model full flow. The line resistances are used to represent the actual pipes, fittings, and test article of an installation. The values from test data used in the input file for the model were activation valve setting, interface pressure, temperature, and mass flowrate. All of these input quantities are for both the LOX system and LH2 system.

The next three sections of the input file used test data to determine steady-state model conditions at a middle flowrate level, low flowrate level, and flowrate at time zero, respectively. The test data values used were activation valve setting, interface pressure, and mass flowrate for each of these sections.

The final section of the input file used in the analysis was the schedules for run tank bottom pressure and activation valve setting. These schedules are time dependent and control the simulation as it steps in time from beginning to end. The schedules contain design points at which you wish the model to operate. These design points were taken from previous test data. The number of design points in the schedules can be as many or as few as needed. Many design points should be scheduled for time periods in

which large changes in bottom pressure or valve setting occur. Fewer design points are needed for time periods in which bottom pressure or the valve setting is near constant. The model interpolates values from the schedule for time steps in between design points.

4.3.2 Sensitivity Methodology

The run time of a single simulation was approximately twenty minutes making analysis by Monte Carlo simulation impractical. The method used to do the sensitivity analysis was a forward-differencing finite-difference approach to obtain a numerical derivative, an example of which is

$$\frac{\Delta W}{\Delta X_1} \approx \frac{W_{X_1+\Delta X1, X2,\ldots,X_j} - W_{X1, X_2,\ldots,X_j}}{\Delta X_1} \tag{4-2}$$

where W is mass flowrate and X represents the particular input of interest [4]. After doing an analysis of all the inputs for the comparison runs, only flowrate and valve position had sensitivities that were not negligible, and these sensitivities were only important for the full flow section of the input file. The sensitivities of the valve schedule and bottom tank pressure schedule were considered negligible for the full range of the model. An individual schedule point only influenced the model during the time between the points previous and subsequent to the schedule point of interest. Therefore, no generalization could be made as to the sensitivity of the model to an individual schedule point. Table 4-1 gives a summary of the input parameters examined and the model's sensitivity to each.

Table 4.1 Model Input Sensitivities

Model Section	Input	LH2 Sensitivity	LOX Sensitivity	Units
Full Mass Flowrate	Valve Position	-2.25	-2.75	$(lb_m/sec)/\%_{open}$
	Mass Flowrate	1.0	1.0	$(lb_m/sec)/ lb_m/sec$
	Interface Pressure	0	0	$(lb_m/sec)/lb_f/in^2$
	Temperature	0	0	$(lb_m/sec)/R$
Mid Mass Flowrate	Valve Position	0	0	$(lb_m/sec)/\%_{open}$
	Mass Flowrate	0	0	$(lb_m/sec)/ lb_m/sec$
	Interface Pressure	0	0	$(lb_m/sec)/lb_f/in^2$
Low Mass Flowrate	Valve Position	0	0	$(lb_m/sec)/\%_{open}$
	Mass Flowrate	0	0	$(lb_m/sec)/ lb_m/sec$
	Interface Pressure	0	0	$(lb_m/sec)/lb_f/in^2$
Time=0	Valve Position	0	0	$(lb_m/sec)/\%_{open}$
	Mass Flowrate	0	0	$(lb_m/sec)/ lb_m/sec$
	Interface Pressure	0	0	$(lb_m/sec)/lb_f/in^2$
Schedules	Valve	NA	NA	$(lb_m/sec)/\%_{open}$
	Tank Bottom Pressure	NA	NA	$(lb_m/sec)/lb_f/in^2$

4.4 Calibrated Model

The data used for calibration was LOX system test 10A and LH2 system test 19D. Both of these tests had near constant tank bottom pressure with the mass flowrates controlled by the activation valve settings. Since the mass flowrates were controlled by the valve settings, all other cases predicted with the model should have mass flowrates controlled in a similar manner. The mass flowrates were modeled for an approximate time of twenty seconds at which point the LH2 reached a steady-state and the LOX test was complete. Plots of the test data versus the model are shown in Figure 4.3 for the LH2 system and 4.5 for the LOX system. Plots of the transient sections of both tests are given in Figures 4.4 and 4.6.

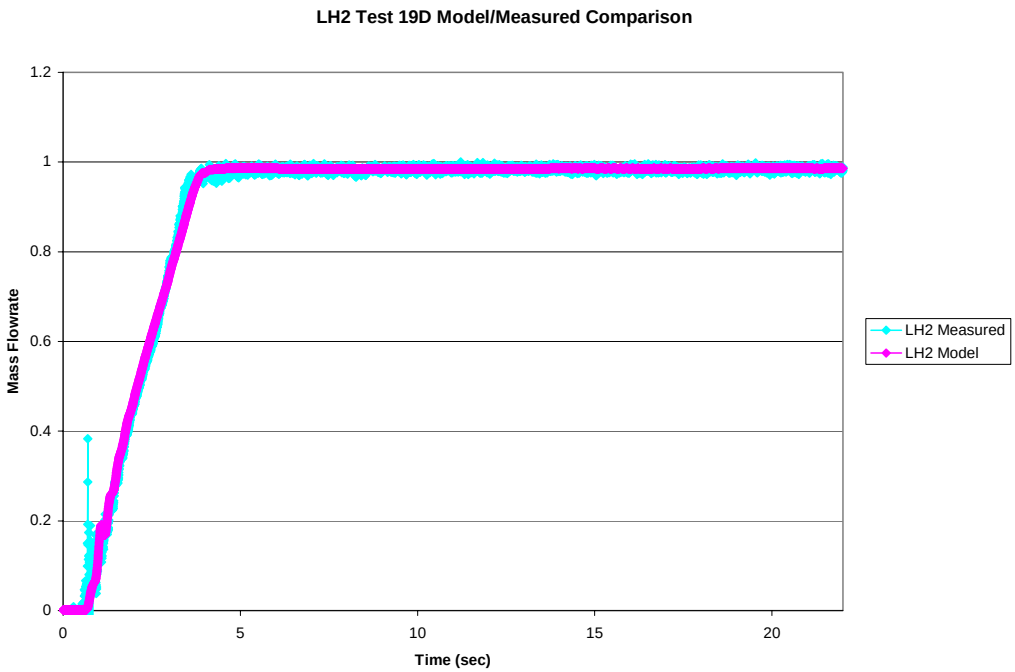

Figure 4.3 LH2 Test 19D Model/Measured Comparison

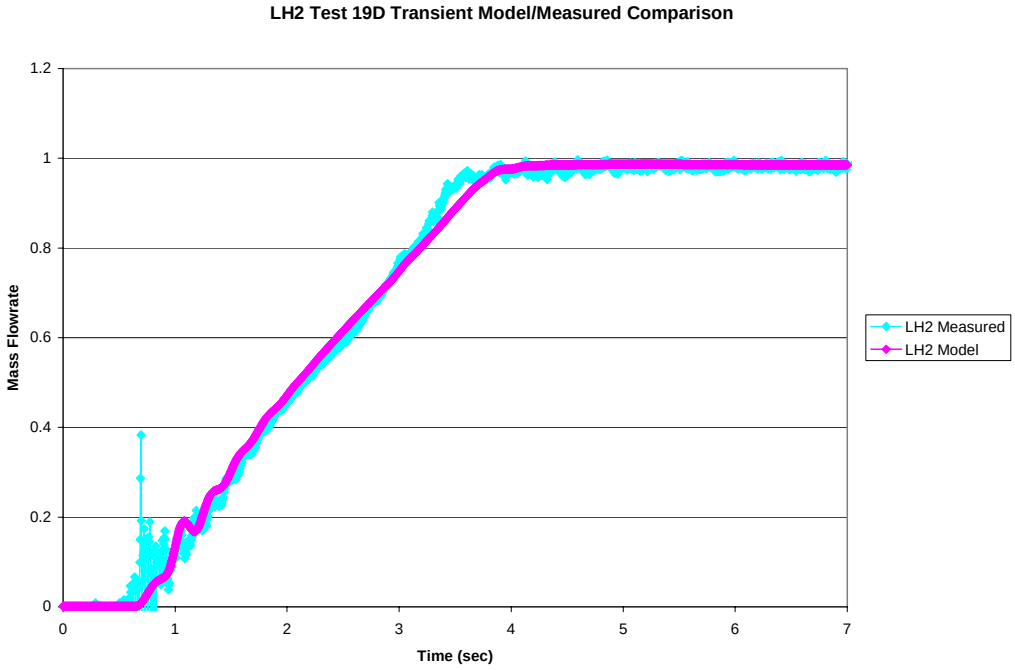

Figure 4.4 LH2 Test 19D Transient Model/Measured Comparison

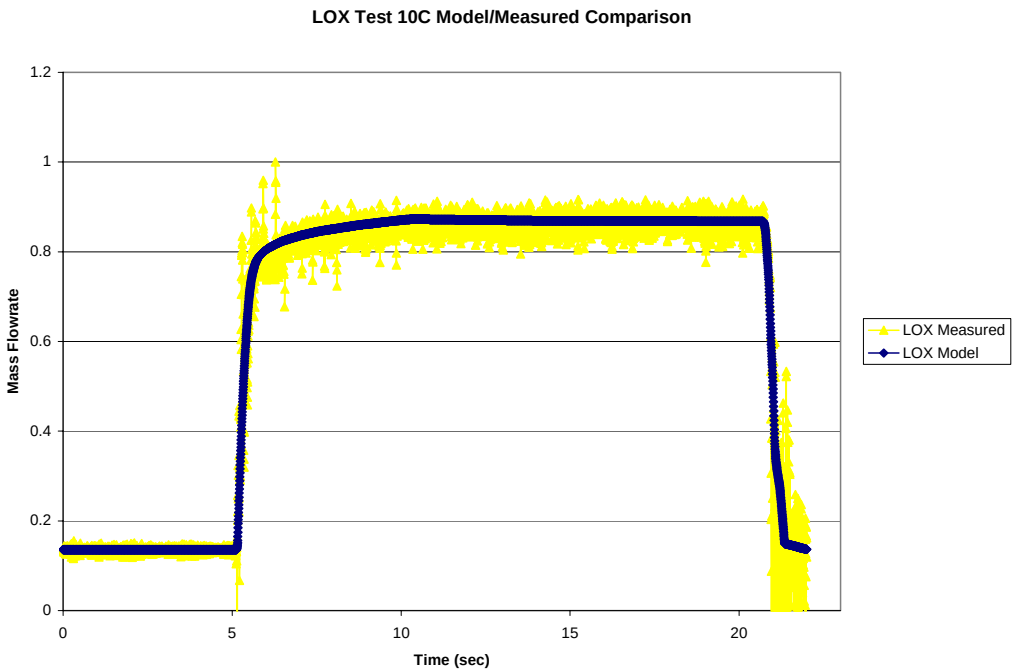

Figure 4.5 LOX Test 10C Model/Measured Comparison

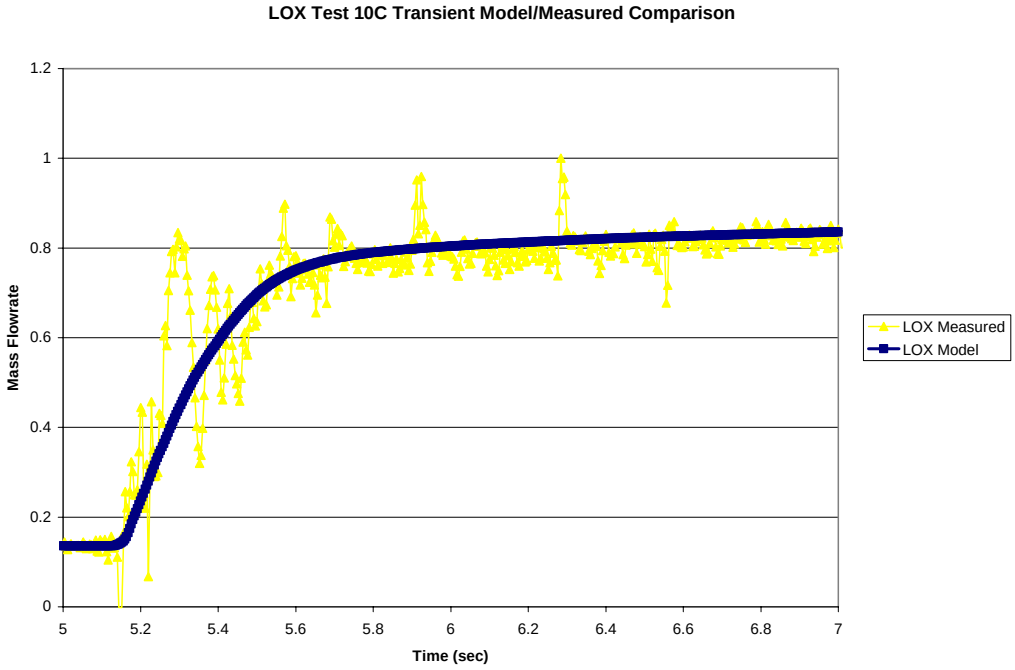

Figure 4.6 LOX Test 10C Transient Model/Measured Comparison

A comparison error will be used to visualize the differences between the calibration test data and the model predictions. Comparison error, E, is defined as the difference between the measured value, D, and the predicted value of the model, S [4]

$$E = D - S \tag{4-1}$$

Comparison errors for the calibration runs are given in Figure 4.7 for the LH2 system and Figure 4.9 for the LOX system. Comparison errors for the transient sections of each calibration run are given in Figures 4.8 and 4.10.

The next chapter will discuss an uncertainty analysis methodology suitable for a general case of a calibrated model. Chapter 6 will use this general methodology to quantify a simulation uncertainty for the calibrated model used in this study. The simulation uncertainty will then be exercised for a new simulation and set of data.

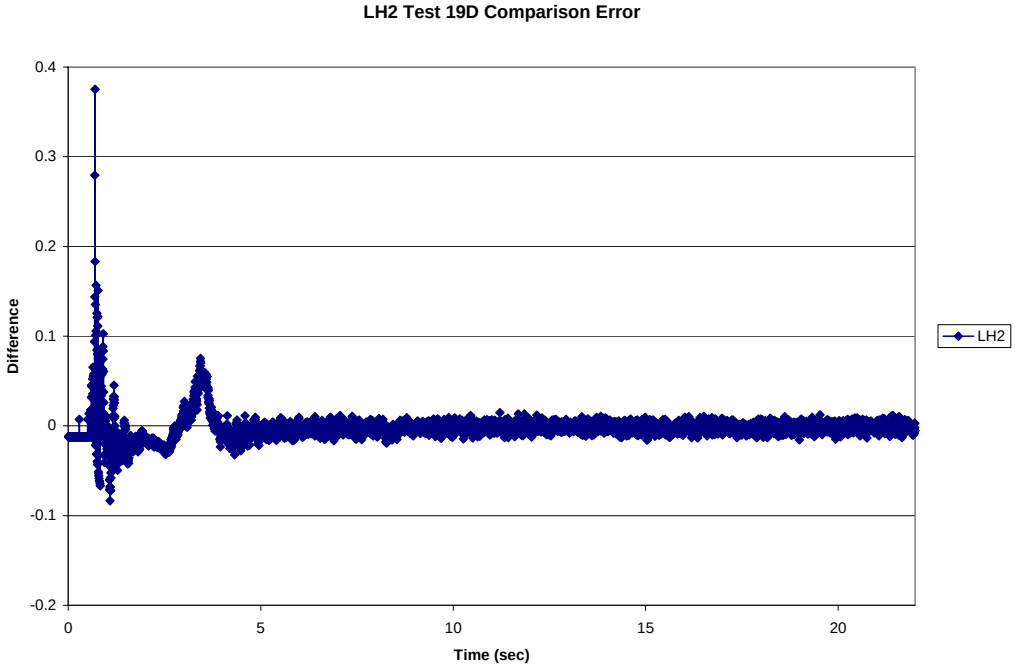

Figure 4.7 LH2 Test 19D Comparison Error

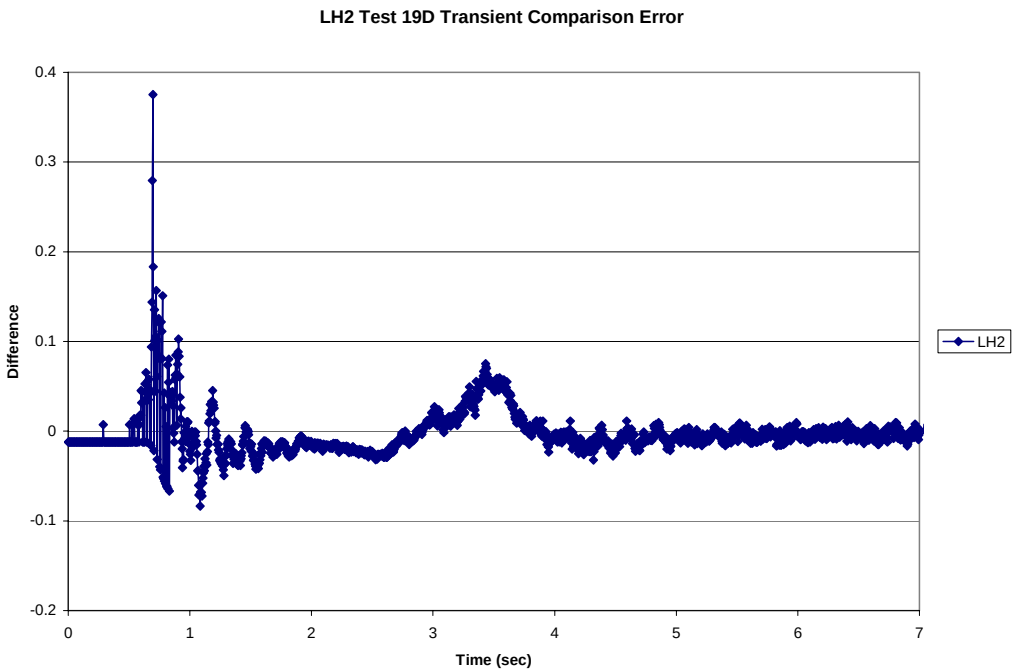

Figure 4.8 LH2 Test 19D Transient Comparison Error

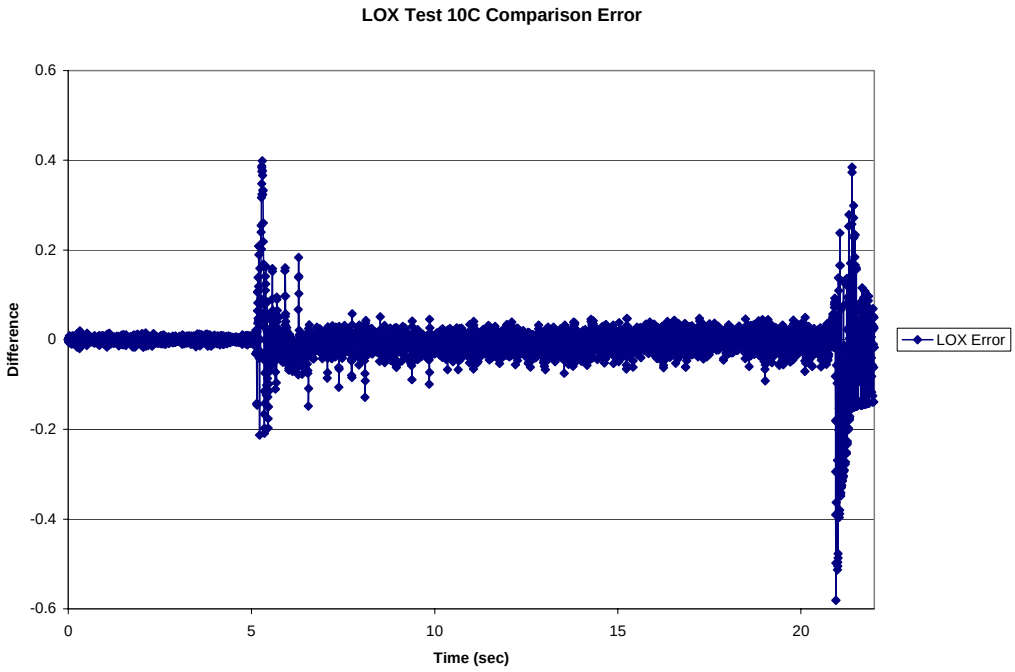

Figure 4.9 LOX Test 10C Comparison Error

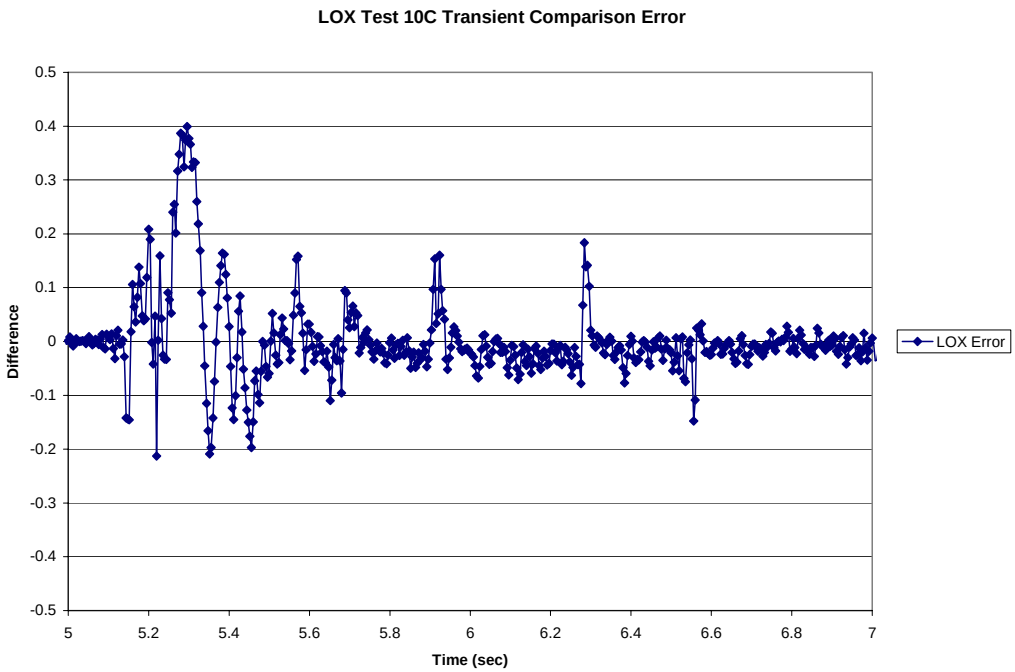

Figure 4.10 LOX Test 10C Transient Comparison Error

CHAPTER V

MODELING UNCERTAINTY METHODOLOGY

This chapter will present a general methodology that quantifies the effects of calibrating a model against calibration data. First, the uncertainty of the data that the model is calibrated against is defined as

$$U_D = 2\sqrt{s_D^2 + b_D^2} = 2b_{Cal} \tag{5-1}$$

where all of the random uncertainty is fossilized in the data used to calibrate the model. Including this fossilized random uncertainty with the systematic uncertainty results in the data uncertainty of, $2b_{Cal}$. (The random uncertainty is included here for a general case, but random uncertainty was considered negligible in the data for this study.)

5.1 Simulation Uncertainty

Model uncertainty will be referred to as simulation uncertainty for the rest of this chapter to be consistent with current nomenclature [4]. Simulation uncertainty is given as

$$U_S^2 = U_{SN}^2 + U_{SPD}^2 + U_{SMA}^2 \tag{5-2}$$

where U_{SN} is the simulation numerical solution uncertainty, U_{SPD} is the simulation modeling uncertainty arising from using previous experimental data, and U_{SMA} is the simulation modeling uncertainty arising from modeling assumptions [4]. Simulation numerical solution uncertainty is often a factor in large field problems, such as a CFD

solution, but for this study U_{SN} is negligible due to its limited number of calculations. The uncertainty of the input data to the model is the source of U_{SPD}, but all of this uncertainty is theoretically replaced by $2b_{Cal}$ in the calibration process; therefore,

$$U_{SPD} = U_D = 2b_{Cal} \tag{5-3}$$

so that

$$U_S^2 = (2b_{Cal})^2 + U_{SMA}^2 \tag{5-4}$$

Since a model calibration is a calibration over a range, the calibrated model will probably differ from the calibration data in some areas. U_{SMA} will take care of this, but it is not known how to quantify U_{SMA} until a simulation result is compared with the calibration data.

From equation (4-1), comparison error is defined as E=D-S. The comparison error, E, is the resultant of all the errors associated with the experimental data and the errors associated with the simulation. Its uncertainty is defined as

$$U_E^2 = \left(\frac{\partial E}{\partial D}\right)^2 U_D^2 + \left(\frac{\partial E}{\partial S}\right)^2 U_S^2 + 2\frac{\partial E}{\partial D}\frac{\partial E}{\partial S}U_{DS} \tag{5-5}$$

U_{DS} is the term that takes into account any correlation between the uncertainties in the experimental data and the simulation. For the calibrated model

$$U_E^2 = U_D^2 + U_S^2 - 2(4)b_{DS} \tag{5-6}$$

where

$$b_{DS} = b_{Cal}^2 \tag{5-7}$$

Now making the appropriate substitutions into equation (5-6) will result in

$$U_E^2 = (2b_{Cal})^2 + (2b_{Cal})^2 + U_{SMA}^2 - 8b_{Cal}^2 \quad (5\text{-}8)$$

or

$$U_E^2 = U_{SMA}^2 \quad (5\text{-}9)$$

Theoretically U_{SMA} would equal to zero for a perfect model. Since U_{SMA} is not known beforehand, U_E in equation (5-9) is not known. The approach taken to determine U_{SMA} is to define a validation uncertainty as

$$U_{Val}^2 = U_E^2 - U_{SMA}^2 = 0 \quad (5\text{-}10)$$

The comparison error, E, from equation (4-1), is expected to be zero with an uncertainty of zero (U_{Val}) because of the calibration process. Therefore, any variation of |E| away from zero will be an indication of U_{SMA}. Hence

$$U_S^2 = (2b_{Cal})^2 + (|E|)^2 \quad (5\text{-}11)$$

or

$$U_S = \sqrt{(2b_{Cal})^2 + (|E|)^2} \quad (5\text{-}12)$$

U_S will be the uncertainty of the use of the model to predict the results of a similar test. If the predicted test will be run with the same equipment, in the same facility, and with the same operating procedure, then the systematic uncertainties between the calibrated model and the predicted test, the b_D's, will be correlated and will cancel out in any comparison between the prediction and actual test results. This effect will become more clear in the next section.

5.2 Model Validation

To complete a validation of the model for another test, D_2, equation (5-1) becomes

$$U_{D_2} = 2\sqrt{s_{D_2}^2 + b_{D_2}^2} \tag{5-13}$$

and the model uncertainty is

$$U_S^2 = (2b_{Cal})^2 + (|E|)^2 \tag{5-14}$$

Now the new comparison error is defined as

$$E_2 = D_2 - S \tag{5-15}$$

with the comparison error uncertainty defined as

$$U_{E_2}^2 = U_{D_2}^2 + U_S^2 - 2(4)b_{D_2S} \tag{5-16}$$

Therefore, substituting for U_{D_2} from equation (5-13) and U_S from equation (5-14) gives

$$U_{E_2}^2 = (2s_{D_2})^2 + (2b_{D_2})^2 + (2b_{Cal})^2 + (|E|)^2 - 8b_{D_2S} \tag{5-17}$$

Substituting for b_{Cal} from equation (5-1) gives

$$U_{E_2}^2 = (2s_{D_2})^2 + (2b_{D_2})^2 + (2b_D)^2 + (2s_D)^2 + (|E|)^2 - 8b_{D_2S} \tag{5-18}$$

If the validation test and calibration test have different sources of systematic uncertainty, b_{D_2S} will be zero and

$$U_{E_2}^2 = (2s_{D_2})^2 + (2b_{D_2})^2 + (2b_D)^2 + (2s_D)^2 + (|E|)^2 \tag{5-19}$$

However, if the validation test and the calibration test have correlated systematic uncertainties so that

$$b_{D_2} = b_D = b_{corr} \tag{5-20}$$

then

$$b_{D_2S} = b_{corr}^2 \tag{5-21}$$

and

$$U_{E_2}^2 = (2s_{D_2})^2 + (2b_{corr})^2 + (2s_D)^2 + (2b_{corr})^2 + \left(|E|\right)^2 - 8b_{corr}^2 \tag{5-22}$$

or

$$U_{E_2}^2 = (2s_{D_2})^2 + (2s_D)^2 + \left(|E|\right)^2 \tag{5-23}$$

If E_2 is less than U_{E_2}, for either the correlated or uncorrelated cases above as applicable, then no additional adjustments to the model are feasible. If E_2 is greater than U_{E_2}, adjustments to the model should be made and the entire calibration process should be repeated until the desired level of E_2 is obtained. The next chapter will apply the simulation uncertainty and model validation methodologies to a new set of test data referred to as the comparison run data.

CHAPTER VI

COMPARISON TESTS

6.1 Simulation Uncertainty

This chapter will use an additional set of test data referred to as comparison runs to apply the general model uncertainty methodology given in the previous chapter. The data used as a comparison for the calibrated model uncertainty analysis was LOX test 9B and LH2 test 19A. Both of these tests were similar in setup and duration to the calibration data. Test 9B used liquid nitrogen in the LOX system while LH2 was again used in the LH2 system. The LOX system test durations were approximately 20 seconds, and the LH2 system tests were approximately 60 seconds. The start-up region is time 5-7 seconds for the LOX system and time 0-7 seconds for the LH2 system.

Equation (5-12) is used for the simulation uncertainty of the comparison run

$$U_S = \sqrt{(2b_{Cal})^2 + (|E|)^2} \tag{5-12}$$

where E is the comparison error from the calibration runs and b_{Cal} is the venturi calibration uncertainty. The comparison error is given in Figures 4.7 and 4.8 for the LH2 calibration test and in Figures 4.9 and 4.10 for the LOX calibration test. The comparison error varies with time for each test. The values are smaller during the initial low-flow and final high-flow steady-state regions of the test and larger during the transient region. From equation (5-1), b_{Cal} is

$$b_{Cal} = \sqrt{s_D^2 + b_D^2} \tag{6-1}$$

As discussed in chapter 3, there was negligible random uncertainty in these IPD activation tests. Therefore, b_{Cal} is only the systematic uncertainty, b_D, from the venturi flowrate uncertainty. This flowrate uncertainty varies with flowrate, and the values of the uncertainty, $2b_D$, are given in the Table 3.3 for different flowrate ranges for all fluids used in the activation tests. For the simulation uncertainty, b_D will vary with the predicted flowrate.

The model was run with the simulation uncertainty applied, and the model was compared to the data. The plots of the full run for the LH2 system are given in Figures 6.1, 6.2, and 6.3. Figure 6.1 displays the full range of the uncertainty for the model and data. The flowrate uncertainty was over 100 % before the transient section because the ΔP measurements of the venturi were very low in the low-flow range. Plotting LH2 modeling with a more reasonable scale that does not include unrealistic values less than zero gives Figure 6.2. The LH2 system transient section is displayed in Figure 6.3. The plots of the full run for the LOX system are given in 6.4, 6.5, and 6.6. Figure 6.4 shows that flowrate uncertainty was over 100 % in the low-flow range because, as in the LH2 system, the ΔP measurements of the venturi for the LOX system very low. Figure 6.5 plots the data with a more reasonable scale that does not include unrealistic values less than zero. The transient section is given in Figure 6.6.

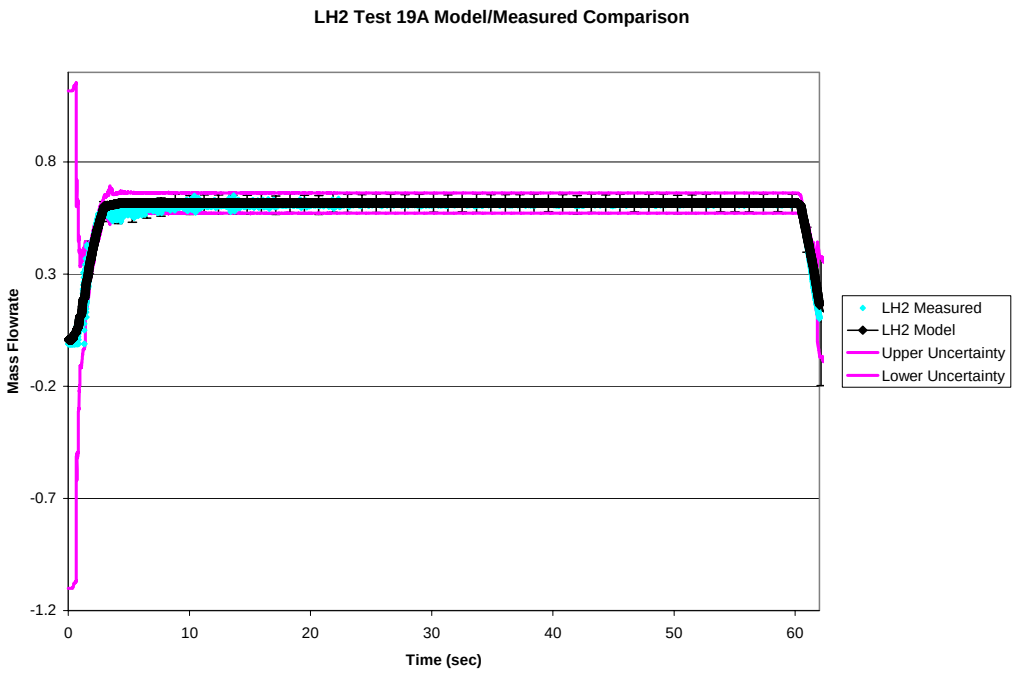

Figure 6.1 LH2 Test 19A Model/Measured Comparison with Uncertainty Full Range

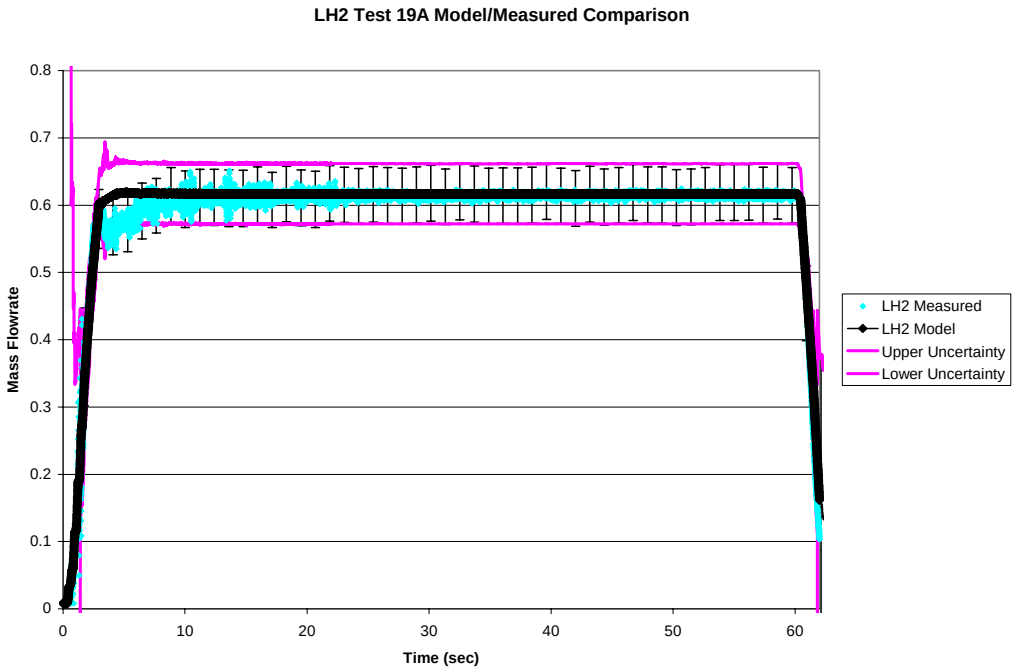

Figure 6.2 LH2 Test 19A Model/Measured Comparison with Uncertainty

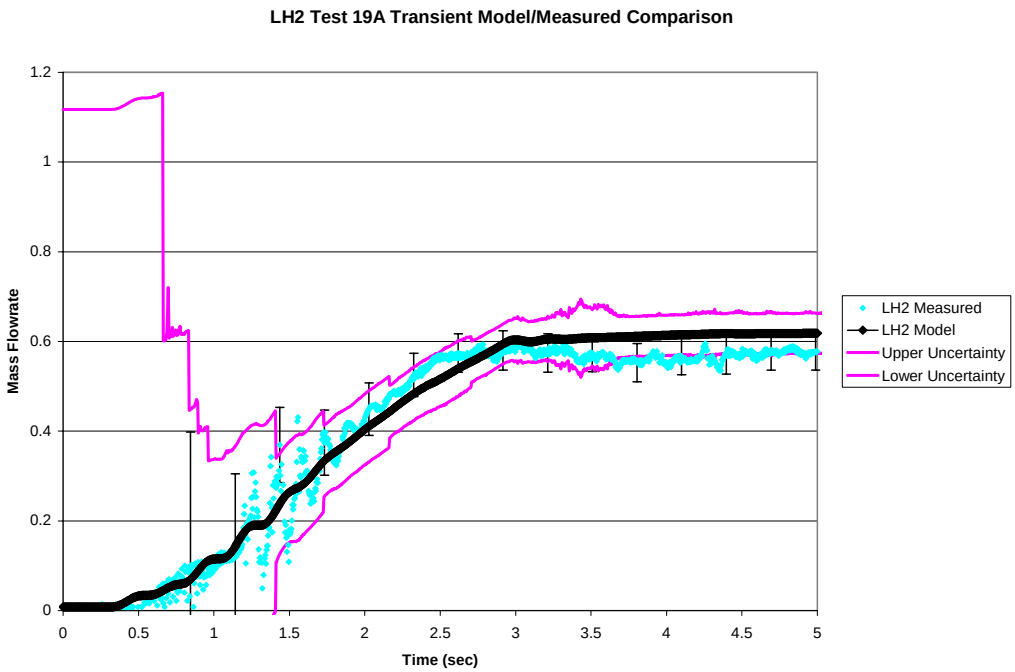

Figure 6.3 LH2 Test 19A Transient Model/Measured Comparison with Uncertainty

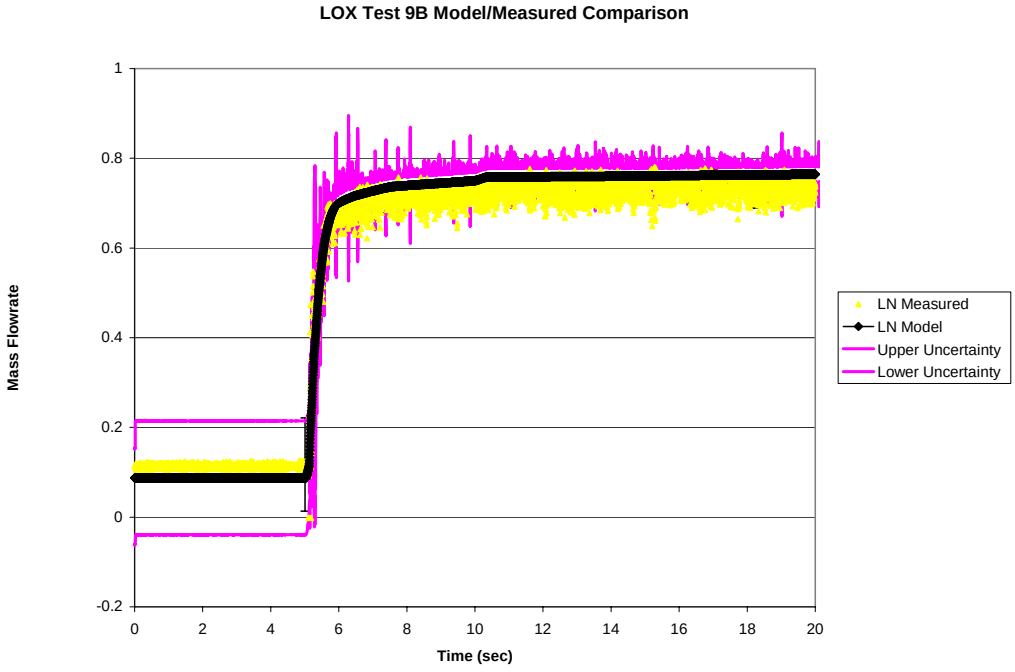

Figure 6.4 LOX Test 9B Model/Measured Comparison with Uncertainty Full Range

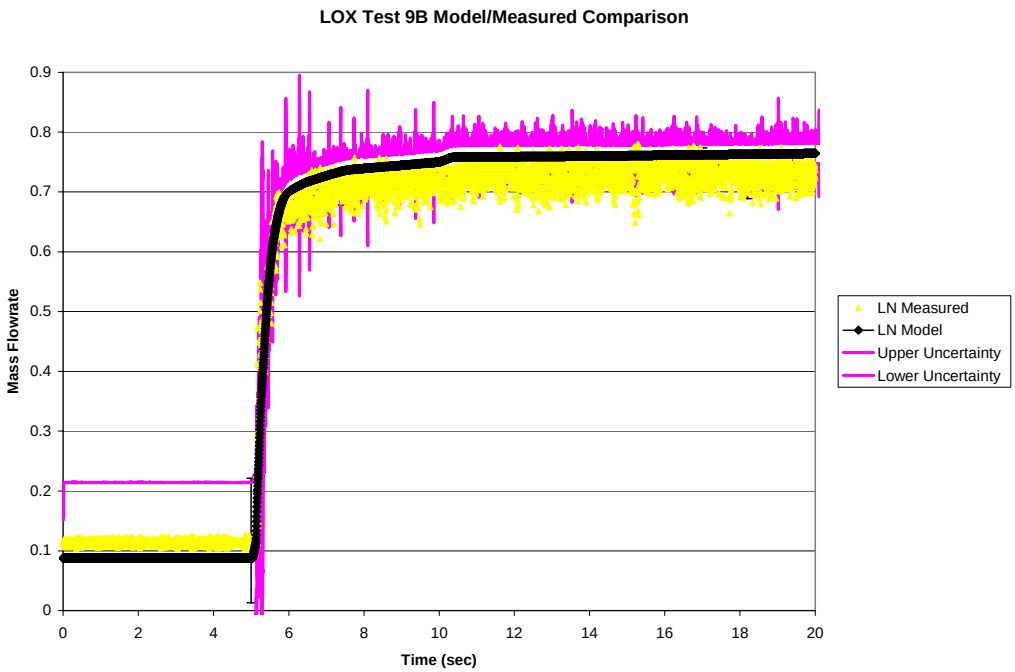

Figure 6.5 LOX Test 9B Model/Measured Comparison with Uncertainty

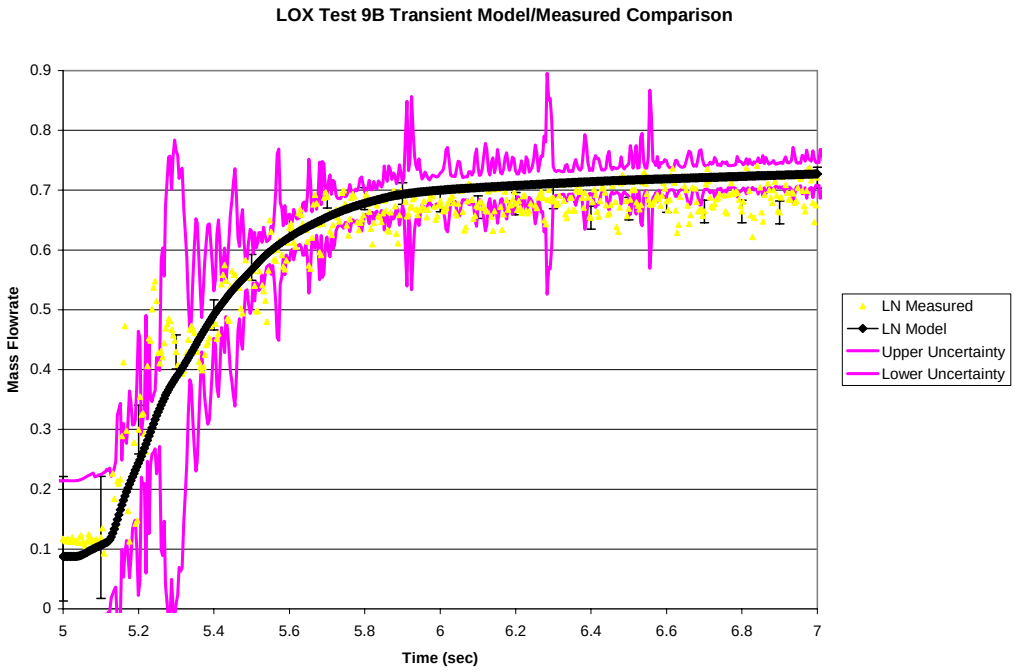

Figure 6.6 LOX Test 9B Transient Model/Measured Comparison with Uncertainty

The comparison run LH2 system test data fell within the predicted uncertainty bands for the model. The only point for which this was not true was the beginning of the high-flow steady-state section of the test. This was due to a phenomenon in the test that was not recorded in the data. It has been speculated that a purge or bleed valve may have opened during that time causing the system pressure loss and drop in flowrate. Therefore, it can be seen that the model cannot match something that is a variation in the operation of the test away from the calibration operation.

The comparison run LOX system test data did not fall within the predicted uncertainty bands for the model as well as the LH2 data did. The data covers the lower uncertainty band shown in the steady state section of the test. This problem was most likely due to LN being used as the test liquid instead of LOX. The model was calibrated with LOX as the fluid, and the comparison model used LN as the fluid. This caused a higher simulation flowrate than was measured. However, the general shape of the test data was matched. It is expected that the comparison would have been better if LOX had been used as the test liquid. Although, even with the different fluid, the difference in the comparison for the high flow steady state region was about 8 % as compared to the simulation uncertainty of 5 %.

6.2 Simulation Validation

The comparison error for the comparison runs will be examined to determine the validation of the comparison run simulation. For the second data set, D_2, the comparison error is given by equation (5-15).

$$E_2 = D_2 - S \tag{5-15}$$

The comparison error uncertainty is for a model that has correlated uncertainties with the calibration data. This correlation requires using equation (5-23)

$$U_{E_2}^2 = (2s_{D_2})^2 + (2s_D)^2 + \left(\left|E\right|\right)^2 \tag{5-23}$$

Since the tests were determined to have no random uncertainty

$$U_{E_2} = \left|E\right| \tag{6-2}$$

If the model is valid for predicting future runs, it is expected that the comparison error, E_2, will fall within the range of $\pm|E_1|$. The comparison error, E_2, is shown in Figures 6.7 and 6.9 for the full comparison runs and in Figures 6.8 and 6.10 for the transient regions.

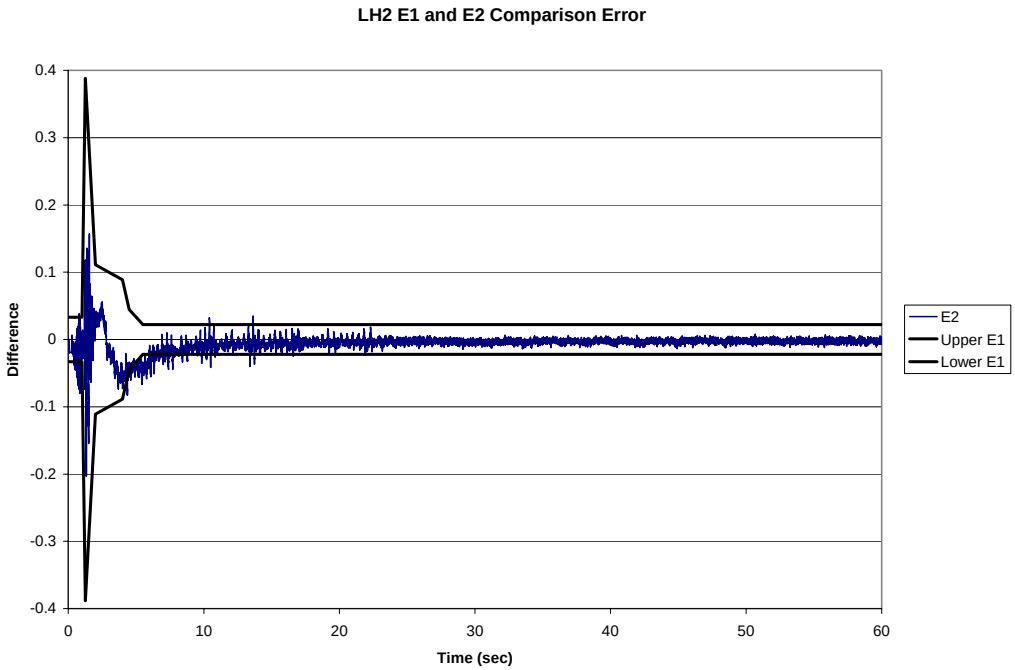

Figure 6.7 LH2 E_1 and E_2 Comparison Error

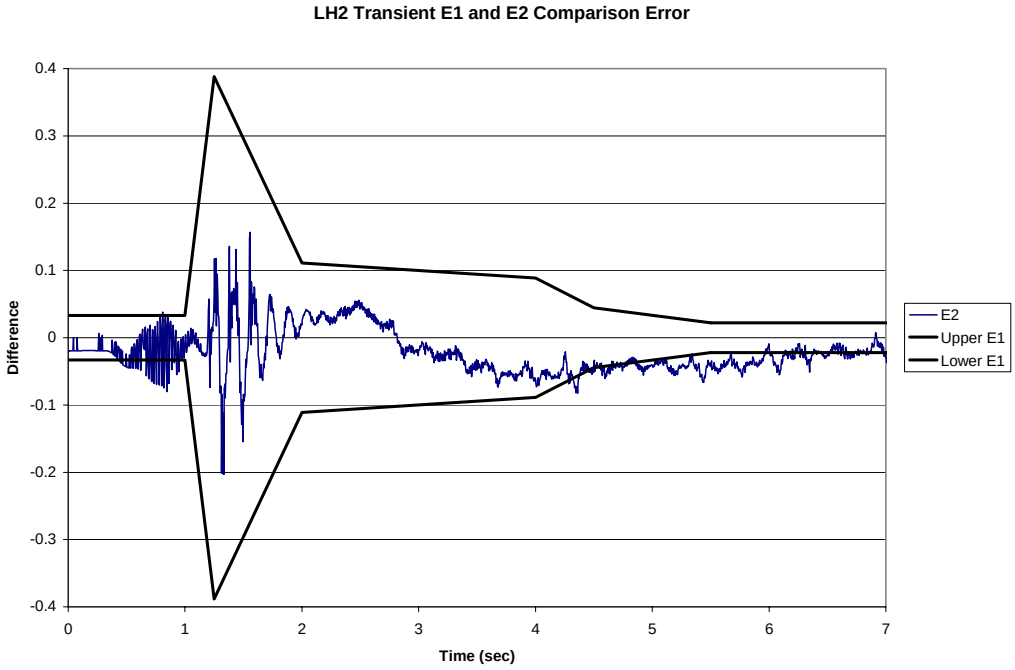

Figure 6.8 LH2 Transient E_1 and E_2 Comparison Error

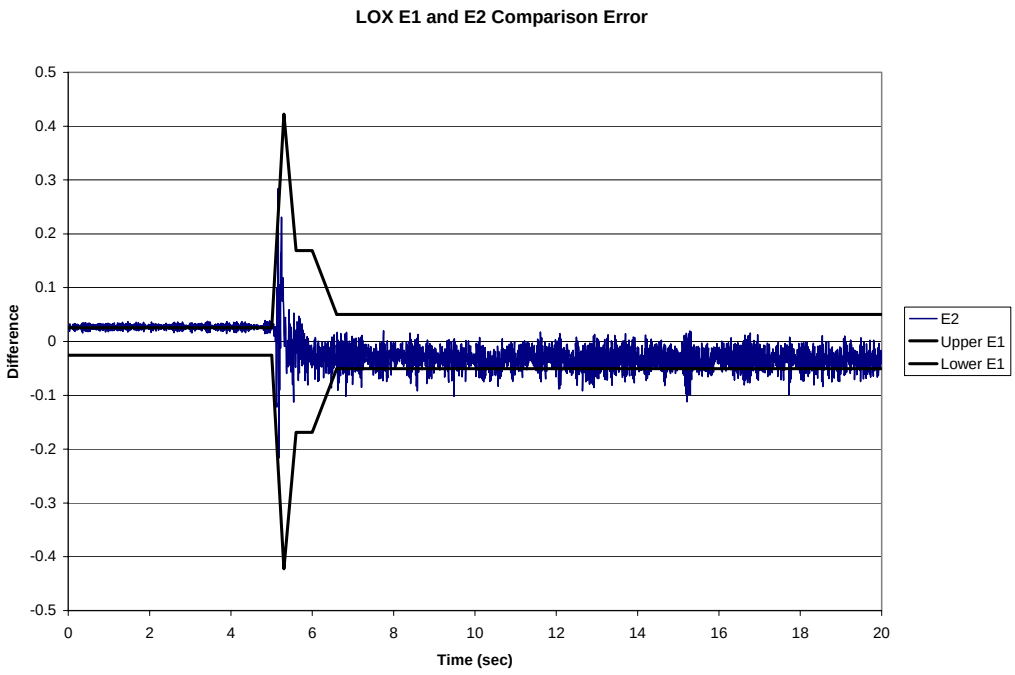

Figure 6.9 LOX E_1 and E_2 Comparison Error

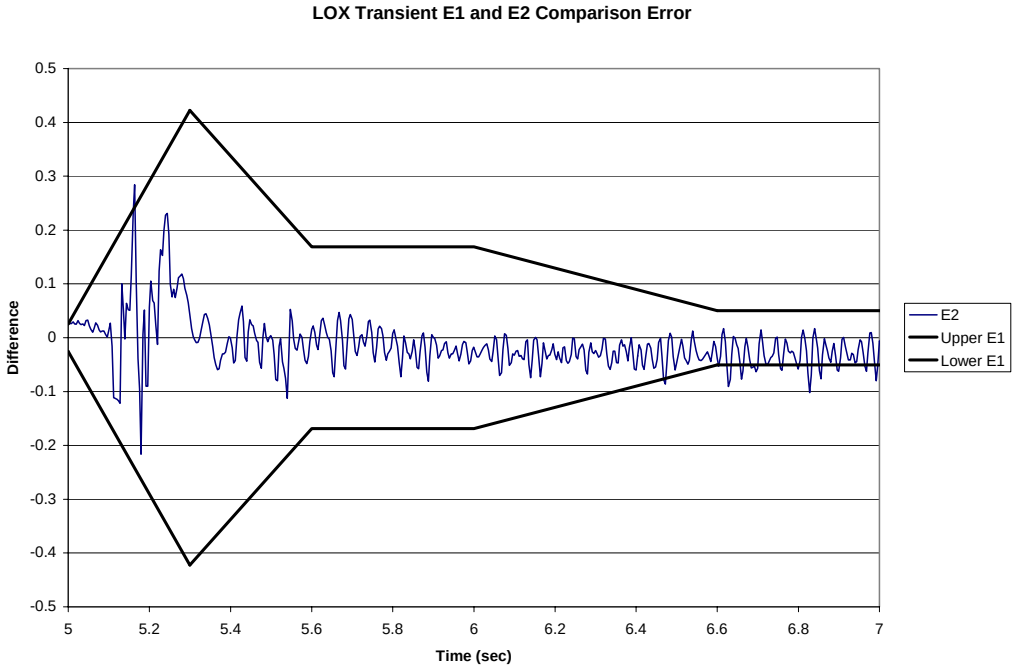

Figure 6.10 LOX Transient E_1 and E_2 Comparison Error

From the previous plots it is seen that E_2 basically falls within the range of E_1. There are very small sections of E_2 that do not fall within the range. These discrepancies were explained in the description of the comparison runs at the end of section 6.1. The discrepancies resulted from phenomenon occurring in the comparison run data that were not part of the calibration data.

CHAPTER VII

CONCLUSIONS

A method to determine the simulation uncertainty of a calibrated model was developed. An analysis of the experimental calibration data was conducted as part of the simulation uncertainty. The Coleman and Stern model validation process was adapted to help formulate the simulation uncertainty methodology required [13]. This methodology was then applied to the model when it was used to predict comparison test results.

The uncertainty analysis of the experimental data was done using methodology described in Steele and Coleman [5]. The uncertainty of the experimental data was the uncertainty of the venturi flow meters used to measure the mass flowrate. This uncertainty was dominated by the ΔP measurement of the venturi. The uncertainty of the venturi was acceptable during the transient and high flowrate steady-state regions of the tests. However, at low flowrates before the transient section began, the uncertainty was over 100 %. This was due to the ΔP measurement being very low. To correct this problem at the lower flowrates a pressure transducer with a smaller range would be needed.

Comparison error was used as a way to quantify all the errors associated with the simulation that could not be directly quantified. These errors in conjunction with the venturi uncertainty were the two components of the overall simulation uncertainty. The

comparison error was large during the transient sections and small during the steady-state sections. It is expected that each time the model goes through a subsequent calibration process, the comparison error will become smaller and smaller.

The process of calibrating a model each time new data is available is logical for the work that is done at NASA Stennis E-1 test facility. Due to the fact that no two engine test series are the same, making one model to encompass all possibilities is impractical. The model uncertainty methodology in this study fits this process of a calibrated model that is constantly "tweaked." This tweaking leaves the user with a calibrated model that can be used to predict the next test condition. A comparison of the model prediction and the next run then shows if additional corrections (calibration) need to be made. As a model is recalibrated over and over during a test series, the unknown uncertainty quantified by the comparison error should decrease. If there are enough tests and recalibrations, the comparison error should eventually come very close to being zero. This would leave only the test data uncertainty from the venturi, which is the best that could ever be achieved since the model is calibrated to the data.

The methodologies developed in this study will help Stennis and Marshall to more accurately measure and model cryogenic flows for the IPD program. These same methodologies can be applied to any future experimental tests that use a similar instrumentation and installation. Also the simulation uncertainty methodology can be applied to a wide variety of models that are calibrated to test data. Future experimental and modeling work will both benefit by reducing the risk to the test article through the use of the uncertainty analysis detailed in this study.

REFERENCES

[1] Marshall Space Flight Center, "Next Generation Propulsion Technology: Integrated Powerhead Demonstrator," NASA Facts, FS-2005-01-05-MSFC, 2005.

[2] International Organization for Standardization, *Guide to the Expression of Uncertainty in Measurement*, ISO, Geneva, 1995.

[3] American Society of Mechanical Engineers (ASME)., *Test Uncertainty*, PTC 19.1-1998, ASME, New York, 1998.

[4] Coleman, H. W., and Steele, W. G., *Experimentation and Uncertainty Analysis for Engineers*, 2nd Edition, Wiley, New York, 1999.

[5] Steele, W.G., and Coleman, H. W., "Experimental Uncertainty Analysis," Chapter 19, "Mathematics," *CRC Handbook of Mechanical Engineering*, 2nd Ed., CRC Press, Florida, 2005.

[6] Taylor, R. P., Hodge, B. K., and Steele, W. G., "Series Piping System Design Program with Uncertainty Analysis," *Heating/Piping/Air Conditioning*, Vol. 65, 1993.

[7] Taylor, R. P., Luck, R., Hodge, B. K., and Steele, W. G., "Uncertainty Analysis of Diffuse-Gray Radiation Enclosure Problems," *Journal of Thermophysics and Heat Transf*er, Vol. 9, 1995.

[8] American Institute of Aeronautics and Astronautics (AIAA)., "Guide for the Verification and Validation of Computational Fluid Dynamics Simulations," AIAA G-077-1998, 1998.

[9] Coleman, H. W., "Some Observations on Uncertainties and the Verification and Validation of a Simulation," *Journal of Fluids Engineering*, Vol. 125, 2003.

[10] Chamra, L. M., Steele, W. G., and Huynh, K., "The Uncertainty Associated with Thermal Comfort," *ASHRAE Transactions*, Vol. 109, 2003.

[11] Mago, P. J., Chamra, L. M., and Steele, W. G., "A Simulation Model for the Performance of a Hybrid Liquid Desiccant System During Cooling and Dehumidification," *International Journal of Energy Research*, Vol. 29, 2005.

[12] American Society of Mechanical Engineers (ASME)., PTC 61 Verification and Validation in Computational Fluid Dynamics and Heat Transfer, http://cstools.asme.org

[13] Coleman, H. W., and Stern, F., "Uncertainties and CFD Code Validation," *Journal of Fluids Engineering*, Vol. 119, 1997.

[14] Law, Boon-Chaun., "Uncertainty Analysis for Rocket-Based Combined Cycle (RBCC) Systems Testing," Masters Thesis, Department of Mechanical Engineering, Mississippi State University, 2003.

[15] American Society of Mechanical Engineers (ASME)., *Fluid Meters: Their Theory and Application*, 6th Edition, ASME, New York, 1971.

[16] Ellis, C., "Calculation of Key Number, Uncertainty, and Recall Interval for Pressure Transducers," Propulsion Test Directorate, John C. Stennis Space Center, 2004.

[17] Seymour, D. C., *ROCETS User's Manual*, Space Transportation Directorate, Marshall Space Flight Center, 1999.

[18] Geil, T., ROCETS Model, PowerPoint Presentation and Personal Communication, 2005.

[19] Hills, R. G., and Trucano, T. G., "Statistical Validation of Engineering and Scientific Models: Background," Sandia National Laboratories, 1999.

[20] Oberkampf, W. L., DeLand, S. M., Rutherford, B. M., Diegert, K. V., and Alvin, K. F., "Error and Uncertainty in Modeling and Simulation," *Reliability Engineering and System Safety*, Vol. 75, 2001.

[21] Oberkampf, W. L., and Trucano, T. G., "Verification and Validation in Computational Fluid Dynamics," *Progress in Aerospace Sciences*, Vol. 38, 2002.

[22] Rutherford, Brian M., and Dowding, K. J., "An Approach to Model Validation and Model-Based Prediction-Polyurethane Foam Case Study," Sandia National Laboratories, 2003.

APPENDIX A

PRESSURE TRANSDUCER EXCEL SPREADSHEET

PRESSURE TRANSDUCER EXCEL SPREADSHEET

Indicator	Color
Input required from user	Yellow
MSU uncertainty input values	Bright Green
Results	Red Bold

Is this an absolute pressure calculated from a differential pressure measurement?	YES

Input Gain (200 or 300)	300

Input Class (A, B or C)	A

Input Uncertainty From Key # Calculation	2

Input Full Scale Range (psi)	2000

Input Posttest Check Tolerance	mV	V	counts
(mV, V, or counts, otherwise, set to 0)	0.00	0.00	100.00

mV	V	counts
0.1042	0.0313	100.0000

Sensitivity	psi / mV	psi / V	psi / count
	66.667	222.222	0.069

Uncertainty Calculations

Systematic

Elemental Source	B (psi)	Comments
Cal. Lab Transducer Calibrations	5	Transducers after calibration according to uncertainty classification.
Shunt Resistor	2.00	From key # uncertainty.
Facility Calibrations	0.00	Assume negligible.
Drift After Calibration	6.94	Calculated based on sensitivity and post-test check tolerance.
P_{atm} Correction	2.00	Only applies if calculate absolute pressure from differential measurement.
Additional Source?	0.00	Add as needed.
Additional Source?	0.00	Add as needed.
Installation Effects	0.00	Add as needed.

Random	P (psi)	Comments
1	0.00	Must be evaluated for each test.

Summary	psi	
	Pressure	Uncertainty
Systematic	2000	9.01
Random		0.00
Total Uncertainty		9.01